Article

Cancer Cell

Cyto-Immuno-Therapy for Cancer: A Pathway Elicited by Tumor-Targeted, Cytotoxic Drug-Packaged Bacterially Derived Nanocells

Graphical Abstract

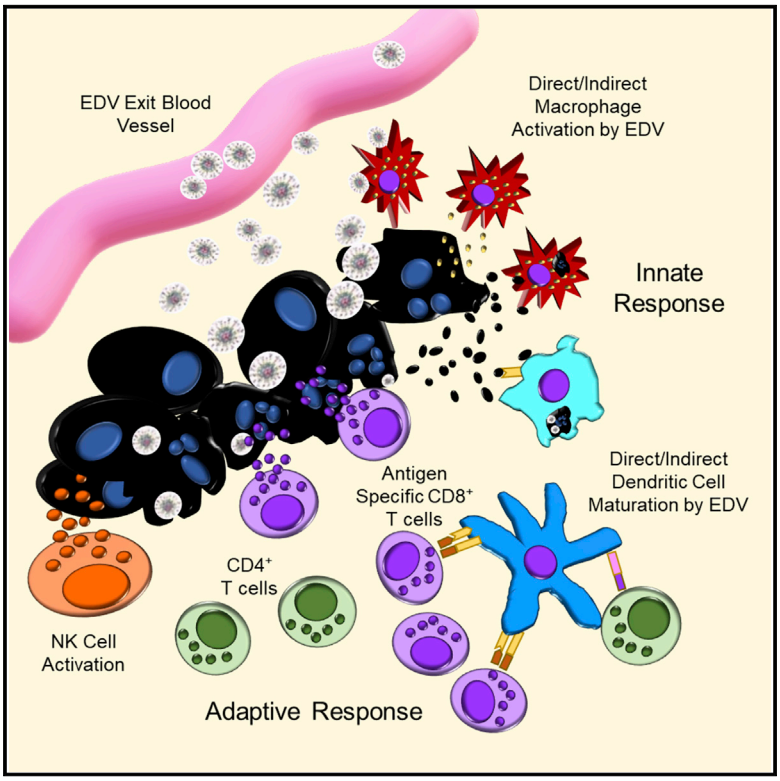

Highlights

- EnGeneIC Dream Vector (EDV) nanocells induce an antitumor innate immune cell response
- EDV treatment results in tumor-specific T cells and an adaptive immune response
- EDV treatment elicits a predominantly Th1 response
- Dual assault on EDV-treated tumors confers long-term survival

Authors

Sharon M. Sagnella, Lu Yang, Gemma E. Stubbs, ..., John Boockvar, Jennifer A. MacDiarmid, Himanshu Brahmbhatt

Correspondence

hbrahmbhatt@engeneic.com

In Brief

Sagnella et al. report the immune modulatory effects of EnGeneIC Dream Vectors (EDVs), bacterially derived nonviable nanocells bearing cytotoxic payloads, in mouse models and human cancer patients. In addition to cytotoxicity, EDVs induce innate and adaptive immune responses to elicit antitumor effects.

Sagnella et al., 2020, Cancer Cell 37, 354–370
March 16, 2020
https://doi.org/10.1016/j.ccell.2020.02.001

CellPress

CellPress

Cancer Cell
Article

Cyto-Immuno-Therapy for Cancer: A Pathway Elicited by Tumor-Targeted, Cytotoxic Drug-Packaged Bacterially Derived Nanocells

Sharon M. Sagnella,[1] Lu Yang,[1] Gemma E. Stubbs,[1] Ebru Boslem,[1] Estefania Martino-Echarri,[1] Katarzyna Smolarczyk,[1] Stacey L. Pattison,[1] Natasha Vanegas,[1] Eva St. Clair,[1] Stephen Clarke,[2] John Boockvar,[3] Jennifer A. MacDiarmid,[1,4] and Himanshu Brahmbhatt[1,4,5,*]

[1]EnGeneIC Ltd, Building 2, 25 Sirius Road, Lane Cove West, Sydney, NSW 2066, Australia
[2]ANZAC Research Institute – Royal North Shore Hospital 38 Pacific Highway, Sydney, NSW 2065, Australia
[3]Northwell School of Medicine, 3rd Floor, 130 East 77th Street, New York, NY 10075, USA?show -"^[fish 0,email]"$60#SYS:EMAILFN$62#>
[4]These authors contributed equally
[5]Lead Contact
*Correspondence: hbrahmbhatt@engeneic.com
https://doi.org/10.1016/j.ccell.2020.02.001

SUMMARY

Immunotherapy has emerged as a powerful new chapter in the fight against cancer. However, it has yet to reach its full potential due in part to the complexity of the cancer immune response. We demonstrate that tumor-targeting EDV nanocells function as an immunotherapeutic by delivering a cytotoxin in conjunction with activation of the immune system. These nanocells polarize M1 macrophages and activate NK cells concurrently producing a Th1 cytokine response resulting in potent antitumor function. Dendritic cell maturation and antigen presentation follows, which generates tumor-specific $CD8^+$ T cells, conferring prolonged tumor remission. The combination of cytotoxin delivery and activation of innate and adaptive antitumor immune responses results in a potent cyto-immunotherapeutic with potential in clinical oncology.

INTRODUCTION

Despite recent advances in cancer immunotherapies (IMTs), their success rates across a variety of tumor types has been limited. A significant proportion of patients who initially demonstrate encouraging tumor regression relapse over time, while other patients lack tumor immunogenicity, and therefore exhibit no initial response (Emens et al., 2017; Oiseth and Aziz, 2017; Sharma et al., 2017). Thus, identification of robust and durable IMT approaches may result in significantly improved clinical outcomes.

To mount an effective antitumor immune response, certain steps must be achieved either spontaneously or therapeutically. First, tumor cell antigens derived *in situ* via tumor cell death, or delivered exogenously, must be taken up by dendritic cells (DCs) (Anguille et al., 2015; Emens et al., 2017; Jung et al., 2018; Mellman et al., 2011). In conjunction with antigen uptake, DCs need to receive proper maturation signals prompting differentiation and enhanced presentation of antigens such that antitumor function, as opposed to tolerance, is promoted (Anguille et al., 2015; Emens et al., 2017; Jung et al., 2018; Mellman et al., 2011; Simmons et al., 2012). Mature, tumor antigen-loaded DCs must then generate antitumor T cell responses, which can occur via the production of tumor-specific cytotoxic T cells, triggering of natural killer (NK), and/or NKT cell responses, and enhancing T helper type 1 (Th1) responses (Emens et al., 2017; Fang et al., 2017; Mellman et al., 2011; Sharma et al., 2017; Zitvogel et al., 2015). Antitumor T cells must finally enter the tumor microenvironment (TME), where immune suppressive signals may be present, and effectively perform their antitumor function (Emens et al., 2017; Mellman et al., 2011). Failure in any of these steps will impede the efficacy of an IMT (Emens et al., 2017; Mellman et al., 2011; Sharma et al., 2017).

Significance

Recent advances in cancer immunotherapy have resulted in durable clinical responses in specific cancers; however, current immunotherapeutic strategies still exhibit low overall response rates. Herein, we report on the mechanism of the cyto-immunotherapeutic function of tumor-targeted nanocells, where a dual assault on the tumor occurs via delivery of a cytotoxin combined with engagement of multiple arms of the immune system. This approach circumvents some of the current pitfalls with immunotherapies by creating an immunogenic tumor microenvironment while also generating immune cell subsets with antitumor function, thereby potentially avoiding primary and/or adaptive resistances that may arise in patients.

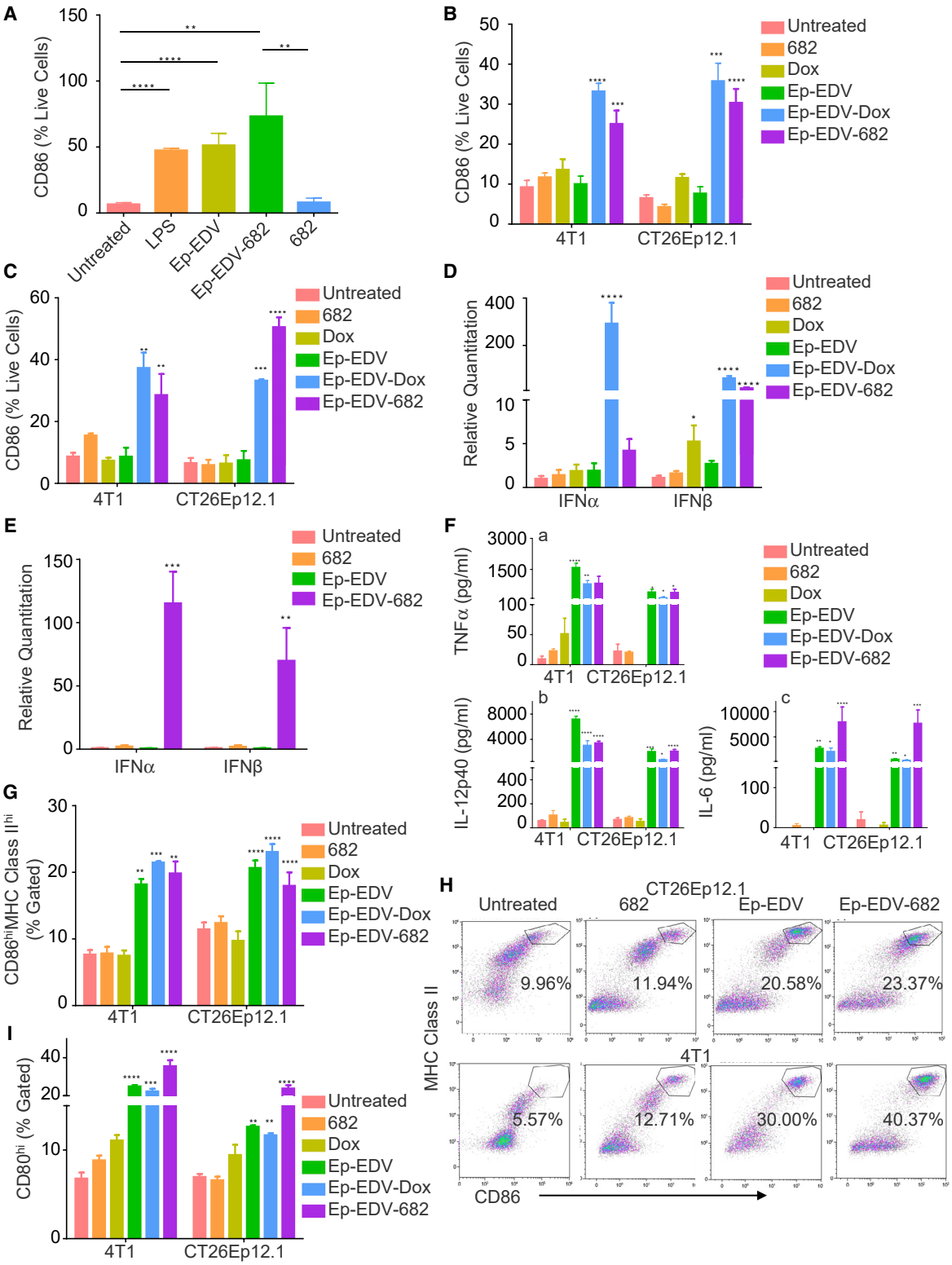

Figure 1. Direct and Indirect EDV Activation of MΦs and DCs

(A–C) CD86 expression analysis by flow cytometry in RAW cells incubated with LPS, Ep-EDV, Ep-EDV-682, or 682 (n = 3) (A); co-cultured with 4T1 (n = 4) or CT26Ep12.1 (n = 3) cells treated with Ep-EDV, Ep-EDV-Dox, Ep-EDV-682, Dox, or 682 (B); or cultured in supernatants from 4T1 (n = 4) or CT26Ep12.1 (n = 3) cells treated with Ep-EDV, Ep-EDV-Dox, Ep-EDV-682, Dox, or 682 (C).

(D and E) PCR quantitation of IFN-α and IFN-β expression in BMDC/4T1 co-cultures (n = 4) (D) or BMDC/CT26Ep12.1 co-cultures (n = 5) (E).

(legend continued on next page)

Currently, the most promising IMT strategies include chimeric antigen receptor T cell (CAR-T) therapy and immunological checkpoint inhibitors (Emens et al., 2017; Mellman et al., 2011; Oiseth and Aziz, 2017; Sharma et al., 2017; Ventola, 2017). CAR-T therapy has produced robust clinical outcomes in "liquid" hematologic cancers, but to date has not produced comparable responses in solid malignancies (D'Aloia et al., 2018). Checkpoint inhibitors, such as CTLA-4 and PD-1/PDL-1, have also shown dramatic clinical results in specific cancers, but overall response rates across different cancers remains low and immune-related toxicities can be high (Jenkins et al., 2018; Sharpe, 2017).

We have developed the EnGeneIC Dream Vector (EDV), a bacterially derived delivery system consisting of nonviable nanocells 400 ± 20 nm in diameter that can be packaged with a cytotoxic drug, small interfering RNA, or microRNA and targeted to tumor cell surface receptors via attachment of bispecific antibodies on their surface (MacDiarmid et al., 2007a, 2009). After intravenous administration, they are retained in the vascular system due to their size, but then rapidly extravasate into the tumor via the tumor-associated leaky vasculature (MacDiarmid et al., 2007b). Tumor cell receptor engagement via the associated bispecific antibody results in macropinocytosis into endosomes and release of the payload via intracellular degradation in the lysosomes (MacDiarmid et al., 2007b; Sagnella et al., 2018). The safety of these nanocells has been demonstrated in three phase I clinical trials with over 1,000 doses administered in various end-stage cancer patients (Kao et al., 2015; Solomon et al., 2015; van Zandwijk et al., 2017; Whittle et al., 2015). EDVs loaded with the super cytotoxic drug PNU-159682 (682) are currently being evaluated in end-stage cancer patients in a phase I trial and have shown promising safety. Given the bacterial nature of the EDV, the current study aimed to investigate the cyto-immunotherapeutic function of EDV nanocells.

RESULTS

Antitumor Macrophage Polarization, DC Activation, and Maturation Occur in Response to EDV Treatment of Tumor Cells

Because the EDV is derived from *Salmonella typhimurium* bacteria, its outer membrane contains a substantial lipopolysaccharide (LPS) content (MacDiarmid et al., 2007b). The interaction of LPS with macrophages (MΦ) is known to result in activation and M1 polarization. To determine if the EDV elicits a similar phenotypic response, RAW264.7 (RAW) cells were incubated with mouse EpCAM-targeted EDVs containing 682 (Ep-EDV-682) or empty (Ep-EDV) and examined for changes in MΦ phenotype and cytokine production. Direct incubation of Ep-EDV-682 and Ep-EDV with RAW cells elicited significant increases in CD86 expression (a hallmark of antitumor M1 tumor-associated MΦs [TAMs]), likely in response to the presence of LPS on the EDV surface, whereas 682 alone did not induce the same response (Figure 1A) (Dong et al., 2016). A minimum ratio of 500 EDVs:1 cell was required for M1 MΦ activation (Figure S1A). RAW cells also displayed a significant increase in tumor necrosis factor alpha (TNF-α) and interleukin-6 (IL-6) (Figure S1B), pro-inflammatory cytokines responsible for Th1 MΦ polarization (Yuan et al., 2015). More interestingly, mouse tumor cells (4T1 and CT26Ep12.1) treated with Ep-EDV-682 and co-culture with RAW cells also generated a significant increase in CD86 expression (Figure 1B) and IL-6 and TNF-α production (Figures S1C and S1D). Tumor cells treated with Ep-EDVs carrying doxorubicin (Ep-EDV-Dox) but not Ep-EDV, 682, or Dox, were also capable of eliciting an increase in CD86 expression indicating that MΦ activation was not drug specific (Figure 1B). RAW cell viability remained >80% in all treatment groups (Figure S1E). Supernatants of Ep-EDV-drug-treated tumor cells were likewise able to induce M1 MΦ polarization (Figure 1C). To ensure activation in tumor/RAW cell co-cultures was not due to a direct EDV interaction, tumor cells were washed before incubation with RAW cells and washed supernatants were examined for EDV content. Only ~1,000 EDVs/sample were detected in the supernatants, well below the number necessary for direct MΦ stimulation (Figure S1F), while minimal EDV staining on the outer cell membrane was observed after incubation of tumor cells with EDVs for 4 h at 37°C. Effective uptake was confirmed by detection of a substantial amount of EDVs in permeabilized cells (Figure S1G). The above results in combination with the fact that Ep-EDV treatment of tumor cells could not elicit MΦ activation indicate that tumor cell death in response to drug-loaded EDV treatment in addition to direct interaction between EDVs and MΦs, elicits M1 polarization.

Direct incubation of EDV with bone marrow-derived DCs (BMDC) resulted in upregulation of DC maturation molecules CD86 and major histocompatibility complex (MHC) class II, again likely as a result of LPS stimulation (Figures S1H and S1I). BMDC co-incubated with treated tumor cells (4T1 and CT26Ep12.1) were assessed for type 1 interferon production, a well-established mechanism of DC maturation and enhanced antigen presentation vital for their interaction with NK cells and T cells (Simmons et al., 2012) (Figures 1D and 1E). BMDC co-cultured with Ep-EDV-682 but not Ep-EDV- or 682-treated CT26Ep12.1 or 4T1 showed significant increases in interferon α (IFN-α) and IFN-β mRNAs, while treatment of CT26Ep12.1 with Ep-EDV-Dox resulted in a significant increase in IFN-β mRNA. Dox-treated CT26Ep12.1 showed a small, significant increase in IFN-β mRNA (Figure 1D). Tumor cell co-cultures with BMDC also exhibited profound increases in the production of TNF-α, IL-12p40, and IL-6, inflammatory and immunostimulatory cytokines produced by functionally stimulated DCs, in response to Dox- and 682-loaded EDVs (Dudek et al., 2013; Jung et al., 2018) (Figure 1F). Upregulation of MHC class II and the costimulatory molecules CD86 and CD80 indicated that co-incubation of

(F) ELISA analysis of supernatants of BMDC/tumor cell co-cultures TNF-α (a), IL-12p40 (b), and IL-6 (c).
(G–I) Flow cytometric analysis of BMDC/tumor cell co-cultures with 4T1 or CT26Ep12.1 cells treated with Ep-EDV, Ep-EDV-Dox, Ep-EDV-682, Dox, or 682. Quantitation of $CD86^{hi}$ and MHC class II^{hi} (n = 3) (G). Representative density plots of MHC class II and CD86 expression in BMDC co-cultures with CT26Ep12.1 cells and 4T1 cells treated with 682, Ep-EDV, and Ep-EDV-682 (H). Quantitation of $CD80^{hi}$ expression (n = 3) (I). Data represent mean ± SEM and analyzed by one-way ANOVA and Tukey's multiple comparison test. *$p \leq 0.05$, **$p \leq 0.01$, ***$p \leq 0.001$, ****$p \leq 0.0001$.
See Figure S1.

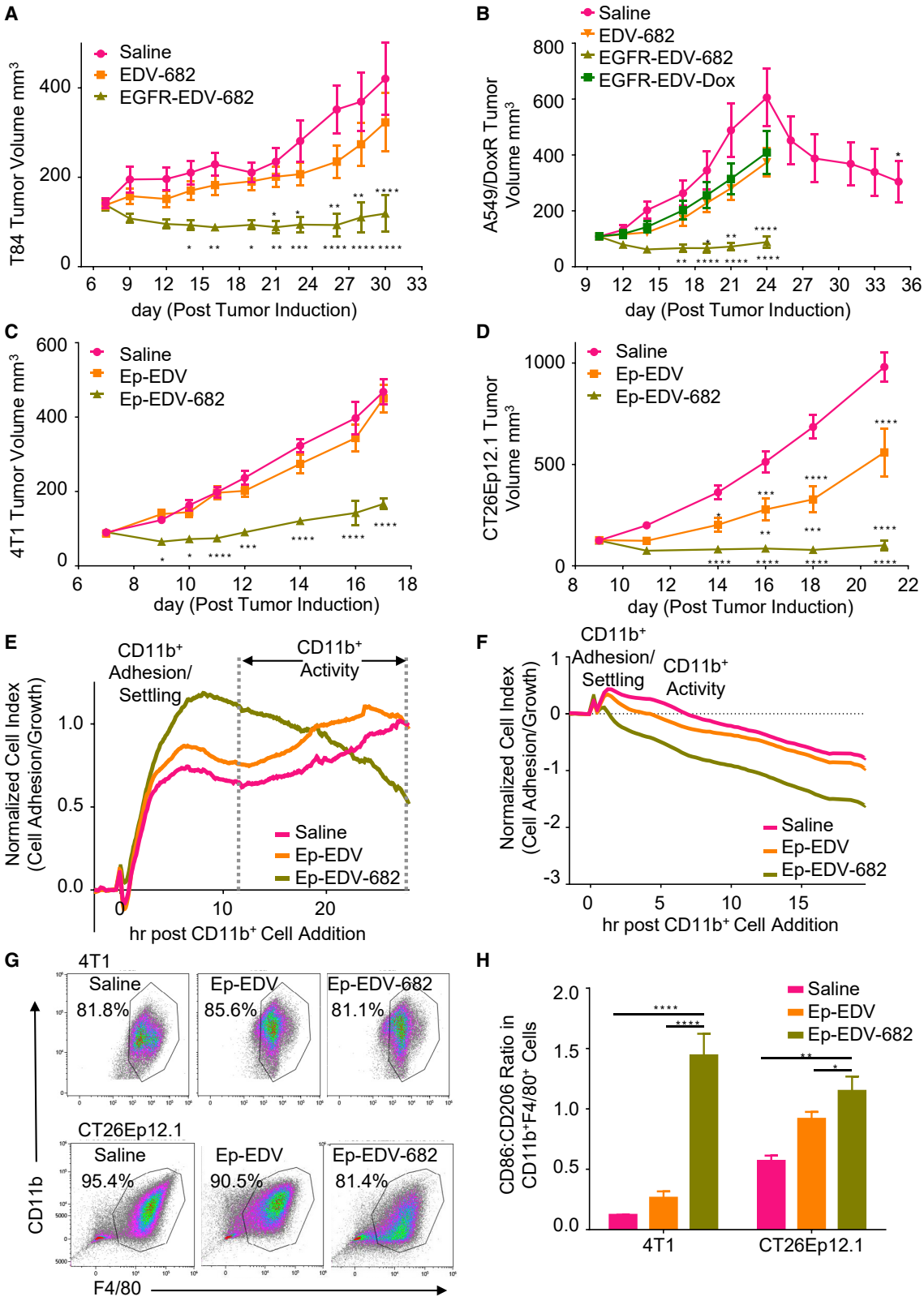

Figure 2. Safe and Effective EDV Delivery of 682 Generates Tumoricidal Innate Immune Cells

(A and B) Tumor growth in response to EDV-682 and EGFR-EDV-682 in BALB/c nude mice T84 xenografts (n = 10) (A) and A549/DoxR xenografts (n = 9) (B). Data represent mean ± SEM and analyzed by a two-way ANOVA and Tukey's multiple comparison test.

(legend continued on next page)

BMDC with Ep-EDV-drug-treated tumor cells results in DC maturation (Figures 1G–1I and S1J). Empty EDV treatment of tumor cells was able to elicit some but not all the hallmarks of DC maturation and, thus, future work is needed to examine this phenomenon. Combined, these results suggest that tumor cells treated with chemotherapy-loaded EDVs are capable of promoting DC maturation into inflammatory and immunogenic DCs, which may be able to elicit potent anticancer immunity through effector T cell priming.

EDVs Can Safely and Effectively Deliver 682

PNU159682, the chemotherapeutic used in the *in vitro* studies, is a metabolite of the anthracycline nemorubicin with half maximal inhibitory concentrations for even drug-resistant cancer cells in the pM range (Quintieri et al., 2005). Because of its extreme potency, it is unable to be used as a free drug clinically due to severe systemic toxicity (Staudacher and Brown, 2017). However, when encapsulated in EDVs, 682 can be effectively delivered to the tumor with few side effects. Ethics approval has been obtained in Australia for the use of 682-loaded EDVs in clinical trials.

Mice treated with Ep-EDV-682 exhibited few side effects as demonstrated by minimal weight loss, little to no fur ruffling, and no appearance of lethargy or hunched postures, which correlates with previous studies involving EDVs carrying different therapeutic payloads (MacDiarmid et al., 2007a; Sagnella et al., 2018) (Figures S2A–S2D).

Efficacy of 682-loaded EDVs targeted to human epidermal growth factor receptor (EGFR), a receptor known to be highly expressed in both cell lines, was examined in athymic BALB/c nude mice bearing T84 and doxorubicin-resistant A549/DoxR human xenografts (Figures 2A and 2B). EGFR-EDV-682 significantly reduced both T84 and A549/DoxR tumor growth, with significant tumor regression achieved in large ($\sim$600 mm^3) A549/DoxR tumors, while EDV-682 did not have the same effect. Significant tumor growth reduction and regression was also observed in BALB/c mice bearing 4T1 and CT26Ep12.1 tumors, respectively, in response to Ep-EDV-682 treatment (Figures 2C and 2D).

EDV Delivery of 682 Generates Tumoricidal $CD11b^+$ Innate Immune Cells

While it is established that the EDV can effectively deliver chemotherapeutics to tumors (MacDiarmid et al., 2007a; Sagnella et al., 2018), our *in vitro* data suggested that they can also generate antitumor MΦ and DC via tumor cell death in response to drug-loaded EDVs. This likely occurs with the release of DAMPs capable of activating and engaging the innate arm of the immune system; however, more in-depth studies are needed to fully characterize the exact mechanism.

To establish if *in vivo* stimulation of the innate immune system within the TME occurred in response to systemic EDV treatment, $CD11b^+$ immune cells were isolated from 4T1 and CT26Ep12.1 mouse tumors treated with saline, Ep-EDV, or Ep-EDV-682 and co-cultured *ex vivo* with their corresponding tumor cells at a 5:1 (effector:target [E:T]) ratio. $CD11b^+$ cells co-cultured with 4T1 cells (Figure 2E) showed an initial adhesion phase, indicated by an increase in cell index followed by an active phase in which cell index increased/decreased steadily if $CD11b^+$ cells were ineffective/effective in killing adherent tumor cells. $CD11b^+$ cells isolated from the tumors of Ep-EDV-682 but not Ep-EDV- or saline-treated mice were effective at killing their corresponding tumor cells. In the CT26Ep12.1 model (Figure 2F), cytolysis was more pronounced in the Ep-EDV-682-treated group beginning within 1 h and falling to 42% viability at 10 h post $CD11b^+$ cell addition. In contrast, it took $\sim$5 and 7 h for cytolysis to begin in the Ep-EDV- and saline-treated groups and viability at 10 h post $CD11b^+$ cell addition was 76% and 86%, respectively.

$CD11b^+$ cells encompass a heterogeneous population of innate immune cells, including but not limited to MΦ, DC, neutrophils, and myeloid-derived suppressor cells; however, greater than 80% of the isolated $CD11b^+$ cells from 4T1 and CT26Ep12.1 tumors were identified as MΦ ($CD11b^+F4/80^+$) (Figures 2G, S2E, and S2F). A small percentage (<10% in CT26Ep12.1 and <3% in 4T1) of the $CD11b^+$ cells were identified as myeloid DC ($CD11b^+CD11c^+F4/80^-$), while the remaining cells ($\sim$5% in CT26Ep12.1 and $\sim$15% in 4T1) were not further phenotyped (Figures S2E and S2F).

Isolated $CD11b^+F4/80^+$ cells were further characterized for the ratio of the M1 marker CD86 to M2 marker CD206. MΦ isolated from 4T1 and CT26Ep12.1 tumors treated with Ep-EDV-682 showed a significant increase in the CD86:CD206 ratio (Figure 2H), which correlated to the increase in cytolytic activity observed in $CD11b^+$/tumor cell co-cultures.

A significant increase in M1/M2 ratio also occurred in both the T84 and A549/DoxR xenografts which correlated to superior tumor cell cytolysis by $CD11b^+$ cells isolated from EGFR-EDV-682-treated A549/DoxR tumors (Figures S2G and S2H).

NK Cells Adopt an Antitumor Phenotype *In Vivo* after EDV Treatment

NK cells are one of the primary effector cells of the innate immune system (Fang et al., 2017; Morvan and Lanier, 2016). Thus, to examine NK cell function, NK cells were isolated from spleens of 4T1 or CT26Ep12.1 tumor-bearing BALB/c mice after treatment with Ep-EDV-682, Ep-EDV, or saline, and co-cultured with their corresponding tumor cells at an E:T of 20:1 (Figures 3A, 3B, and S3A). NK cells of Ep-EDV-682- but not Ep-EDV- or saline-treated mice demonstrated significant and potent cytolysis of target tumor cells. Cytolysis of CT26Ep12.1 cells by NK cells from Ep-EDV-682-treated mice occurred within the first few hours with only 18% target cell viability after 50 h, while

(C and D). Tumor growth in response to Ep-EDV and Ep-EDV-682 treatment in BALB/c mice bearing 4T1 (n = 12) (C) or CT26Ep12.1 tumors (n = 12) (D). Data represent mean ± SEM and analyzed by a two-way ANOVA and Tukey's multiple comparison test.

(E and F) xCELLigence RTCA (normalized cell index versus time) of tumor cell death in response to $CD11b^+$ isolated from 4T1 tumors (E) and CT26Ep12.1 tumors (F) co-cultured with their corresponding tumor cells at a 5:1 (E:T) ratio.

(G) Density plots of flow cytometric analysis of CD11b and F4/80 expression in $CD11b^+$ cells isolated from 4T1 and CT26Ep12.1 tumors.

(H) Ratio of M1($CD86^+$): M2 ($CD206^+$) MΦs in $CD11b^+$ $F4/80^+$ cells isolated from 4T1 and CT26Ep12.1 tumors of CD11b and F4/80 expression (n = 4).

Data represent mean ± SEM and analyzed by one-way ANOVA and Tukey's multiple comparison test. *$p \leq 0.05$, **$p \leq 0.01$, ***$p \leq 0.001$, ****$p \leq 0.0001$. See Figure S2.

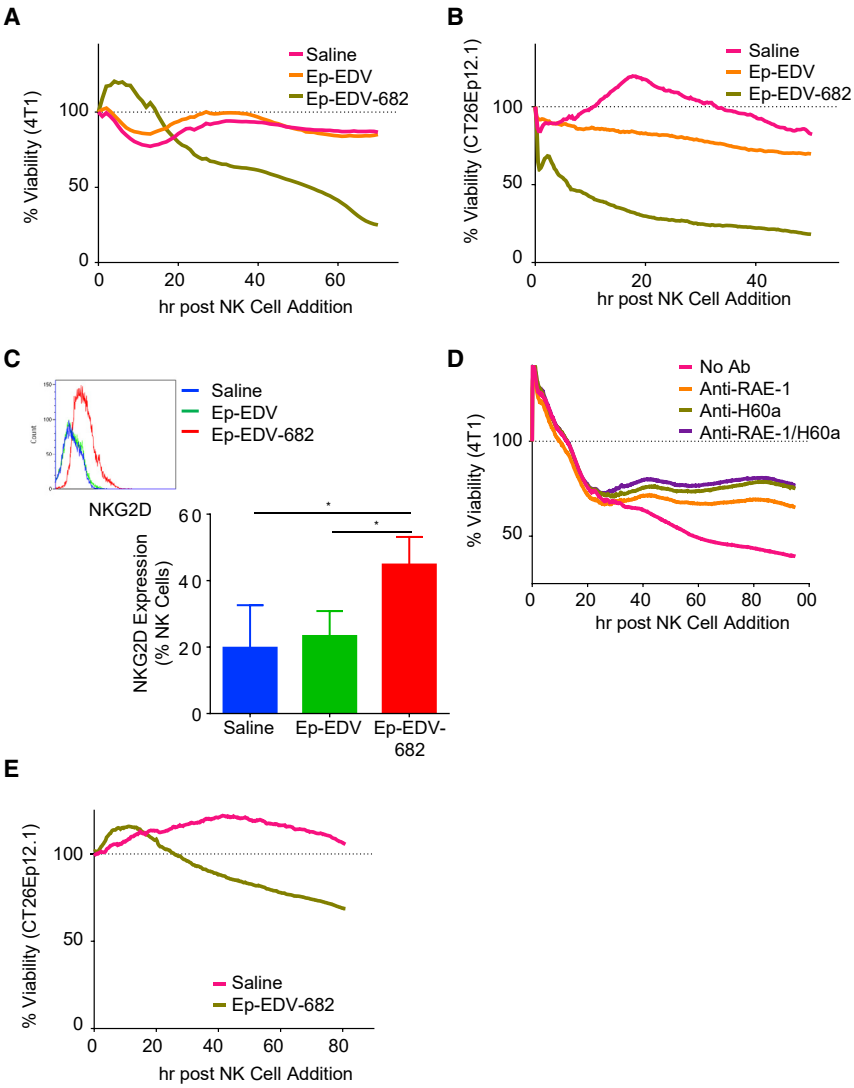

Figure 3. EDV Delivery of 682 Generates Cytolytic NK Cells

(A and B) RTCA (percent viability versus time) of NK cells isolated from spleens of mice bearing 4T1 tumors co-cultured with 4T1 cells (A) and CT26Ep12.1 tumors co-cultured with CT26Ep12.1 cells (B) at a 20:1 (E:T) ratio. Plots represent cell viability over time.

(C) Expression of NKG2D in NK cells within 4T1 tumors determined by flow cytometry (n = 4). Data represent mean ± SEM and analyzed by a one-way ANOVA and Tukey's multiple comparison test.

(D and E) RTCA (percent viability versus time) of NK cells isolated from spleens of Ep-EDV-682-treated 4T1 tumor-bearing mice co-cultured with 4T1 cells at a 20:1 (E:T) ratio in the presence of RAE-1 and/or H60a-inhibiting antibodies (D) and mice bearing CT26Ep12.1 tumors co-cultured with 4T1 cells at a 20:1 (E:T) ratio (E). *p $\leq$ 0.05.

See Figure S3.

Ep-EDV and saline treatment resulted in low level of cytolysis (70%–80% cell viability) in the same time period. In the 4T1 model, NK cells from Ep-EDV-682-treated mice decreased target cell viability to ~36% after 70 h, while those from saline- or Ep-EDV-treated mice maintained ≥90% target cell viability. NK cells isolated from the A549/DoxR and T84 tumor models demonstrated similar cytolytic profiles to the immunocompetent models (Figures S3B and S3C).

NK cells require two distinct stages, priming via release of activating cytokines or expression of activating receptors by the target cell and triggering via the co-engagement of an additional NK-activating receptor specific to stressed cells followed by release of the contents of their cytolytic granules, thus killing target tumor cells (Fang et al., 2017; Sabry and Lowdell, 2013). NK cells ($CD45^+CD3^-DX5^+$) in Ep-EDV-682-treated 4T1 tumors had a significant increase in NKG2D expression, an NK-activating receptor important in tumor immunosurveillance (Figure 3C). Upregulation of NKG2D ligands on the tumor cell surface can override NK inhibitory signals triggering tumor cell cytolysis (Morvan and Lanier, 2016). Screening of mouse tumor cell lines for the NKG2D binding ligands RAE-1, H60a, and MULT-1 showed that 4T1 and CT26Ep12.1 had high levels of H60a expression, while 4T1 cells also expressed RAE-1 and MULT-1 (Figure S3D). Antibodies to RAE-1 and H60a were effective in inhibiting NK cytolysis of 4T1 cells, with ~13%, 21%, and 25% inhibition by RAE-1, H60a, or a combination of the two antibodies, respectively (Figures 3D and S3E).

Because both 4T1 and CT26Ep12.1 cell lines contain NKG2D-binding ligands, NK cells primed by Ep-EDV-682 treatment should be able to target both cell types regardless of their source. In fact, NK cells from Ep-EDV-682-treated CT26Ep12.1 tumor showed cross-reactivity against 4T1 cells (Figure 3E). The potent cytotoxicity observed in the two mouse models indicates that Ep-EDV-682 treatment results in changes within the TME, which can induce NK cell priming. The reduction in cytolysis observed with NKG2D ligand blocking indicates that the NKG2D receptor binding to tumor cells is one but likely not the only mechanism by which tumor cell cytolysis is triggered. Further studies are needed to fully elucidate mechanisms of NK triggering in drug-loaded EDV-treated tumors.

EDV Treatment Leads to the Production of Tumor-Specific $CD8^+$ T Cells

We next aimed to determine if DC maturation in response to EDV treatment observed *in vitro* translated to the production of tumor-specific $CD8^+$ cytotoxic T cells *in vivo*. $CD8^+$ T cells isolated from spleens of 4T1 or CT26Ep12.1 mice treated with saline, Ep-EDV, or Ep-EDV-682, were co-cultured with their corresponding tumor cells (Figures 4A and 4B). $CD8^+$ T cells isolated from mice bearing 4T1 and treated with Ep-EDV-682 but not saline or Ep-EDV, exhibited 50% 4T1 cell cytolysis after 30 h (Figures

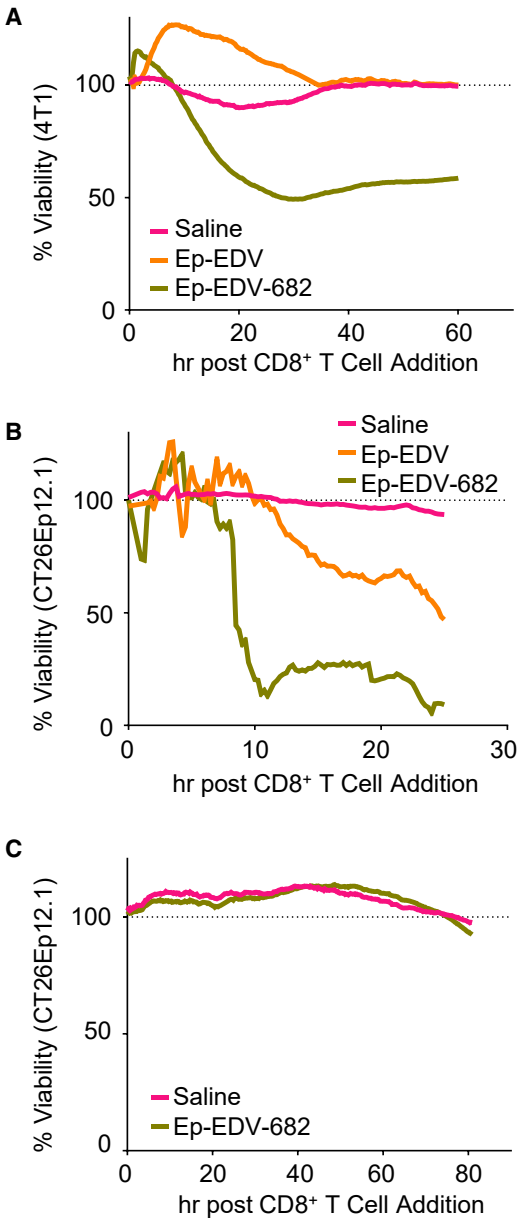

Figure 4. EDV Delivery of 682 Generates Tumor-Specific CD8$^+$ T Cells

(A–C) RTCA (percentage viability versus time) of CD8$^+$ T cells isolated from the spleens of mice bearing 4T1 tumors co-cultured with 4T1 cells (A), CT26Ep12.1 tumors co-cultured with CT26Ep12.1 cells (B), and CT26Ep12.1 tumors co-cultured with 4T1 cells (C) at a 30:1 (E:T) ratio. All plots represent cell viability over time. See Figure S3.

4A and S3F). Similarly, CD8$^+$ T cells isolated from Ep-EDV-682-treated mice bearing CT26Ep12.1 were highly effective in killing CT26Ep12.1 cells, with 81% death after 20 h (Figures 4B and S3G). Ep-EDV but not saline treatment also produced tumor-specific CD8$^+$ T cells in the CT26Ep12.1 model, albeit to a lesser degree, with 40% death after 20 h. To confirm specificity, CD8$^+$ T cells isolated from CT26Ep12.1 tumor-bearing mice were co-cultured with 4T1 cells, with no target cell cytolysis occurring in either saline or Ep-EDV-682-treated samples (Figure 4C).

Activation of Innate and Adaptive Immune Cell Subsets Contribute to EDV Efficacy

682 is highly effective in killing tumor cells, and it was unknown if the action of the drug itself would override any contribution from the antitumor immune cells activated as a result of Ep-EDV-682 treatment.

To examine the role of innate immune cells on efficacy, anti-CD11b and anti-Asialo-GM$_1$ antibodies were used to deplete CD11b$^+$ and NK cells, respectively, *in vivo* followed by Ep-EDV-682 treatment. CD11b is present on all myeloid-derived cells and depletion of CD11b$^+$ cells would include MΦ, DC, MDSC, and some populations of NK cells, while anti-Asialo-GM$_1$ is used for specific NK cell depletion. Clodronate liposomes were administered to specifically deplete MΦs; however, mice were unable to tolerate MΦ depletion combined with EDV treatment, and thus the efficacy of Ep-EDV-682 treatment in MΦ-depleted mice was unable to be examined. CD11b$^+$-depleted mice also exhibited some adverse side effects after EDV treatment (weight loss and ruffled fur). These results suggest a vital role for phagocytic cells in tolerance of systemic EDV administration, which will require further studies.

Anti-Asialo-GM$_1$ or anti-CD11b treatment resulted in ≥98% and ∼70% reduction in NK and CD11b$^+$ cells in the tumors, respectively. Depletion of both CD11b$^+$ and NK cells significantly reduced Ep-EDV-682 efficacy (Figure 5A). CD11b$^+$ cell depletion did not affect tumor growth rate, and no significant difference occurred between CD11b$^+$-depleted mice treated with Ep-EDV-682 and those treated with saline + anti-CD11b$^+$ or saline alone. In contrast, depletion of NK cells resulted in a significant increase in tumor growth rate, and NK cell-depleted mice treated with Ep-EDV-682 showed a significant reduction in tumor size as compared with mice treated with saline + anti-Asialo-GM$_1$. To account for the differences in tumor growth rates, a ratio of Ep-EDV-682:saline tumor volume was calculated (Figure S4A). Following the first Ep-EDV-682 treatment, tumor sizes in mice receiving no antibody were ∼70% smaller than those receiving saline, whereas tumor sizes in CD11b$^+$- and NK cell-depleted mice were only 30%–35% smaller than their saline-treated counterparts. Ep-EDV-682 treatment was least effective in CD11b$^+$-depleted mice, with final tumor sizes being <30% smaller, while final tumor sizes were ∼45% smaller in NK cell-depleted mice as compared with saline. In comparison, in non-depleted mice, Ep-EDV-682 treatment resulted in ∼90% reduction in final tumor size.

The role of T cells in Ep-EDV-682 efficacy were also explored (Figure 5B). T cell depletion in tumors was ≥97% and resulted in a reduction in Ep-EDV-682 efficacy, with CD8 and CD4 depletion having differing effects. No significant difference in tumor size was observed between non-depleted and CD4$^+$ T cell-depleted Ep-EDV-682-treated mice; however, CD4$^+$ T cell depletion slowed tumor growth rate. In contrast, CD8$^+$ T cell depletion resulted in a significant reduction in Ep-EDV-682 efficacy. In the first week of treatment, tumor growth in Ep-EDV-682 T cell-depleted tumors remained relatively stable, with only a slight increase in tumor volume in the Ep-EDV-682-treated CD8$^+$ T cell-depleted group, while non-depleted Ep-EDV-682 tumors continued to decrease significantly in size. By day 16, tumor growth had accelerated considerably in the CD8$^+$ T cell-depleted Ep-EDV-682-treated tumors, while non-depleted Ep-EDV-682 tumor size remained stable. In contrast to CD4$^+$ T cell depletion, CD8$^+$ T cell depletion resulted

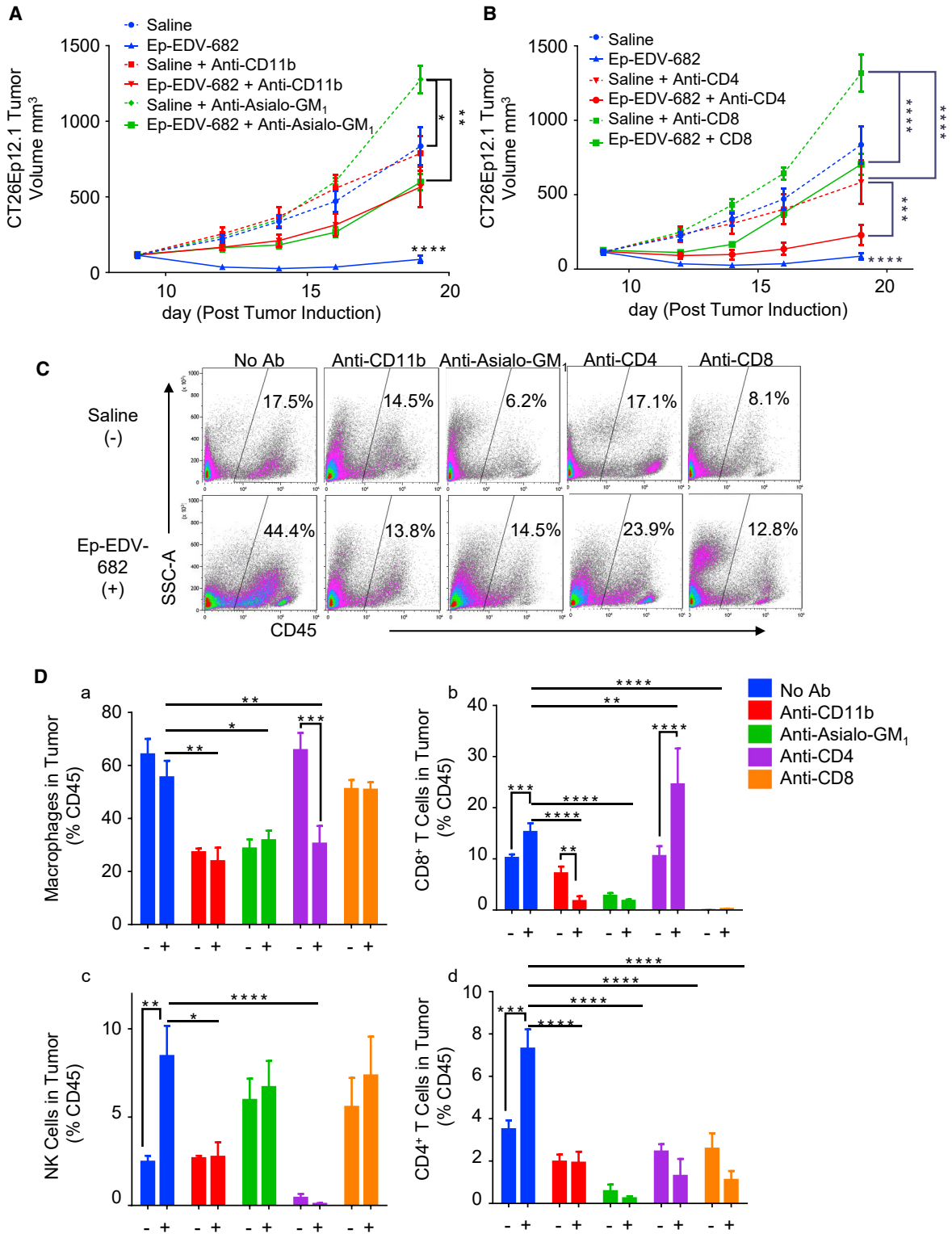

Figure 5. Integrally Connected Roles of Innate and Adaptive Immune Cells in EDV Antitumor Immune Response to EDV Treatment

(A and B) Tumor growth in CD11b$^+$ and NK cell-depleted mice in response to saline and Ep-EDV-682 treatment in BALB/c mice bearing CT26Ep12.1 tumors (n = 8) (A) and CD4$^+$ and CD8$^+$ T cell-depleted mice in response to saline and Ep-EDV-682 treatment in BALB/c mice bearing CT26Ep12.1 tumors (n = 8) (B). Data represent mean ± SEM and analyzed by a two-way ANOVA and Tukey's multiple comparison test.

(C) Flow cytometric density plots of CD45$^+$ cells in saline-treated (−) and Ep-EDV-682-treated (+) CT26Ep12.1 tumors depleted of immune cells using antibodies as indicated.

(legend continued on next page)

in accelerated tumor growth. Thus, the ratio of Ep-EDV-682: saline tumor volume was again examined (Figure S4B). Ep-EDV-682 treatment with CD4 depletion resulted in ~61%–68% reduction in tumor size as compared with saline + anti-CD4. CD8 depletion achieved a maximum reduction in tumor size of ~62% at the end of week 1, with final tumor sizes ~50% smaller than their saline counterparts.

Innate and Adaptive Immune Cell Subsets Have Integrally Connected Roles in the Antitumor Immune Response to EDV

Compared with saline, Ep-EDV-682 treatment was responsible for a significant increase in %CD45$^+$ immune cells infiltrating tumors (Figures 5C and S4C). Following depletion of CD11b$^+$, NK, and CD8$^+$, but not CD4$^+$ T cells, overall immune cell infiltration decreased. CD4$^+$ and NK, but not CD11b$^+$- or CD8$^+$-depleted tumors exhibited an increase in the %CD45 cells in tumors in response to Ep-EDV-682 treatment; however, %CD45 was still significantly less than in non-depleted tumors.

The composition of tumor-infiltrating immune cells demonstrated that Ep-EDV-682 treatment had no effect on %MΦ (CD11b$^+$F4/80$^+$), while it resulted in a significant increase in CD4$^+$ T cells, CD8$^+$ T cells, and NK cells (CD3$^-$DX5$^+$) (Figure 5D). A similar result was seen in the 4T1 tumor model (Figure S4D).

As expected, %MΦ decreased after CD11b$^+$ depletion; however, a decrease in the proportion of CD4$^+$, CD8$^+$, and NK cells in the tumor-infiltrating immune cell population was also observed (Figure 5Da). MΦ, CD4$^+$, CD8$^+$, and NK cell proportions were significantly lower in Ep-EDV-682-treated CD11b-depleted tumors as compared with non-depleted tumors. Ep-EDV-682 treatment could not elicit an increase in immune cell populations as seen in non-depleted tumors and even exhibited a significant decrease in %CD8$^+$ T cells, indicating that CD11b$^+$ cells play an important role not only in efficacy but in recruitment of other immune cells after EDV activation.

NK cell depletion resulted in decreases in MΦ and CD8$^+$ T cell proportions (Figure 5Da and b) and failed to provoke any increase in immune cell populations in response to Ep-EDV-682 treatment. CD4 and CD8 depletion resulted in a decrease in NK cell populations, which further decreased after Ep-EDV-682 treatment (Figure 5Dc). Although CD8 depletion eliminated the effect of Ep-EDV-682 on CD4$^+$ T cell increase, CD8$^+$ T cell numbers still increased after Ep-EDV-682 treatment in CD4$^+$-depleted tumors (Figure 5Db and d). Anti-CD4 treatment caused a significant decrease in the MΦ population in Ep-EDV-682-treated tumors. These results suggest that *in vivo* immune cell activation resulting from EDV treatment involves the coordinated effort of multiple arms of the immune system.

EDV Treatment Increases Chemokine Production and a Predominantly Th1 Cytokine Response within the TME

Cytokine and chemokine production within the TME allows immune cells to effectively communicate with each other to generate a coordinated response that can either be tumor promoting or suppressing (Lee and Margolin, 2011).

The production of the inflammatory chemokines CCL2, CCL3, and CCL5 within the TME is a major determinant of infiltration by immune cells, such as MΦs, antigen-presenting cells (APC), NK cells, and T cells (Allen et al., 2018; Brown et al., 2007; Lanca et al., 2013). Significant increases in the level of all three chemokines were detected after Ep-EDV-682 treatment in CT26Ep12.1 tumors (Figure 6A). CCL3 and CCL5 levels were similarly increased in Ep-EDV-682-treated 4T1 tumors (Figure S5A). Likewise, *ex vivo* CD11b$^+$/4T1 co-cultures with CD11b$^+$ cells isolated from Ep-EDV-682-treated 4T1 tumors exhibited a significant increase in the production of CCL3 as compared with those from saline- or Ep-EDV-treated mice (Figure S5B).

Depletion of CD11b$^+$, NK, and CD8$^+$ T cells resulted in a significant decrease in the levels of all three chemokines in Ep-EDV-682-treated tumors, whereas CD4$^+$ T cell depletion resulted in a significant decrease only in CCL2. Given the overall lower numbers of CD45$^+$ cells in the depleted tumors, lower chemokine and cytokine levels were expected. However, Ep-EDV-682 treatment could not elicit a significant increase in chemokine levels in immune cell-depleted tumors as compared with saline treatment, bar a few exceptions. CD11b-depleted tumors exhibited a decrease in CCL3 and CCL5 levels after following Ep-EDV-682 treatment.

NK cell depletion showed a >95% decrease in CCL3 and CCL5, while CCL2 decreased by ~75%, indicating an important role for EDV-activated NK cells in attracting additional immune cells to the TME. This was supported by the fact that *ex vivo* NK/4T1 co-cultures with NK cells from Ep-EDV-682-treated 4T1 tumor-bearing mice exhibited a significant increase in the production of CCL5 (Figure S5C). Combined, these results point to an important role for innate immune cells, particularly NK cells, in the upregulation of CCL3 and CCL5 in response to EDV treatment *in vivo*, while T cells appear to play a larger role in CCL2 upregulation, possibly through the ability of CD4$^+$ T cells to attract additional MΦ to the microenvironment.

To understand the mechanism by which EDV-triggered immune cell activation occurs *in vivo*, interstitial tumor cytokine levels were examined. In general, Ep-EDV treatment resulted in similar interstitial tumor cytokine and chemokine levels to saline treatment (Figure S5D).

Ep-EDV-682 treatment resulted in a significant increase in IFNα concentration in both tumor models (Figures 6B and S5E), and CD11b$^+$ and NK cell depletion led to a reduction in IFN-α after Ep-EDV-682 treatment. IL-12p40 levels significantly increased in Ep-EDV-682-treated CT26Ep12.1 tumors, and CD11b$^+$, NK, and CD8$^+$ T cell depletion led to little change in IL-12p40 production after Ep-EDV-682 treatment (Figure 6B). Both tumor models exhibited a significant increase in TNF-α within the TME in response to Ep-EDV-682 treatment (Figures S5E and S5F). Depletion of innate and T cells both resulted in TNF-α levels decreasing to that of non-depleted saline tumors (Figure S5F). The most prominent change in cytokine level with

(D) Quantitation of immune cell populations in saline-treated (−) and Ep-EDV-682-treated (+) immune cell-depleted CT26Ep12.1 tumors. MΦ (CD11b$^+$F4/80$^+$) (a); CD8$^+$ T cells (CD3$^+$CD8$^+$) (b); NK cells (CD3$^-$CD49b$^+$) (c); and CD4$^+$ T cells (CD3$^+$CD4$^+$) (d), represented as %CD45$^+$ cells (n = 4). *p ≤ 0.05, **p ≤ 0.01, ***p ≤ 0.001, ****p ≤ 0.0001.
See Figure S4.

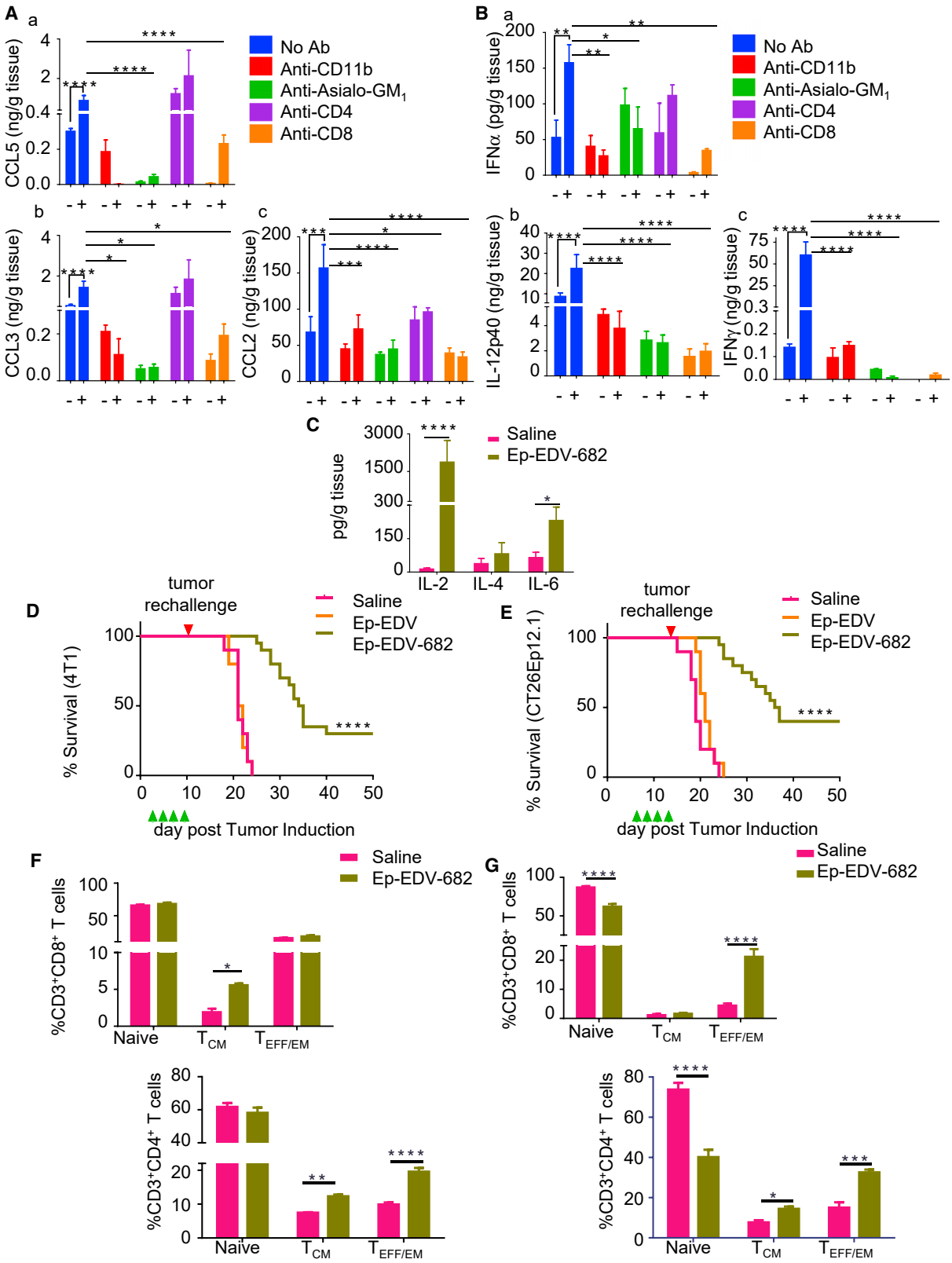

Figure 6. EDV Treatment Results in the Production of Predominantly Th1 Cytokines and Long-Term Survival

(A) Interstitial tumor chemokine concentration of CCL5 (a), CCL3 (b), CCL2 (c) in non-depleted and immune cell-depleted CT26Ep12.1 tumors treated with saline (–) and Ep-EDV-682 (+) (n = 4). Data represent mean ± SEM and analyzed by a two-way ANOVA and Tukey's multiple comparison test.

(legend continued on next page)

Ep-EDV-682 treatment was seen in the CT26Ep12.1 tumors, in which a 500-fold increase in IFN-γ levels occurred (Figure 6B), while a small but significant increase in IFN-γ occurred in the 4T1 tumors (Figure S5E). Again, depletion of innate cells and T cells resulted in a significant decrease in IFN-γ, with NK cell depletion resulting in near zero levels after Ep-EDV-682 treatment (Figure 6B). In Ep-EDV-682-treated CT26Ep12.1 tumors, IL-2 and IL-6 but not IL-4 levels significantly increased (Figure 6C), while significant increases in IL-2 and IL-4 but not IL-6 occurred in 4T1 tumors after Ep-EDV-682 treatment (Figure S5G). IL-1β levels significantly decreased in 4T1 tumors but showed no significant change in the CT26Ep12.1 tumors in response to Ep-EDV-682 (Figure S5H).

EDV Treatment Confers Increased Long-Term Survival, Prolonged Tumor Remission, and Resistance to Tumor Re-challenge

4T1 and CT26Ep12.1 models treated with Ep-EDV-682 exhibited a significant increase in long-term survival, with complete regression in 40% of CT26Ep12.1 and 35% of 4T1 mice and no relapse up to 50 days after initial tumor inoculation (Figures 6D and 6E). Upon re-challenge, 100% of naive control mice formed tumors in both models within 3 days (4T1) and 5 days (CT26Ep12.1) after re-challenge. One hundred percent of saline-treated CT26Ep12.1 mice that survived 5 days after re-challenge formed tumors on the opposite flank, while 0% of the Ep-EDV-682-treated mice, including those that had not completely resolved their initial tumor, formed tumors on the opposing flank. Similarly, 100% of saline- and only 25% of Ep-EDV-682-treated 4T1 mice formed tumors after re-challenge.

T cell population in the spleens of surviving Ep-EDV-682-treated CT26Ep12.1 mice examined on day 50 exhibited significant increases in total T cell numbers, including $CD4^+$ and $CD8^+$ populations (Figure S5I), while no change was observed in 4T1 mice (Figure S5J). In the 4T1 model, no change in naive ($CD44^-CD62L^-$) $CD4^+$ and $CD8^+$ T cells was observed, while there was a significant increase in $CD8^+$ central memory (T_{CM}: $CD44^+CD62L^+$) T cells, $CD4^+$ T_{CM}, and $CD4^+$ effector/effector memory T cells (T_{EFF}/T_{EM}: $CD44^+CD62L^-$) (Figure 6F). In the CT26Ep12.1 model, a significant decrease in naive $CD4^+$ and $CD8^+$ T cells was observed in Ep-EDV-682-treated mice concurrent with a significant increase in $CD4^+$ T_{CM} and both $CD4^+$ and $CD8^+$ T_{EFF}/T_{EM} populations (Figure 6G).

Patient Response to EGFR-EDV-682 in a Case of Stage IV Pancreatic Ductal Adenocarcinoma and EGFR-EDV-Dox in a Case of Recurrent Glioblastoma

Finally, we report on the clinical observation of two different patients undergoing treatment with EGFR-targeted EDVs loaded with a chemotherapeutic demonstrating translation of the preclinical immune activation results to humans. The first is a compassionate case usage of EGFR-EDV-682 treatment in a patient (P1) with stage IV pancreatic ductal adenocarcinoma (PDAC). Even after gemcitabine and FOLFIRINOX, P1 presented with a CA19-9 level of >120,000 kU/L, 3,000 times higher than normal, and an increased C-reactive protein (CRP) level of 64 mg/L.

PDAC cells obtained from resected tumor tissue were found to overexpress EGFR with >200,000 copies per cell (Figures S6A and S6B) in both the head and tail of the tumor. PDAC cells exhibited extreme sensitivity to 682, while having partial to no response to first- and second-line drugs (Figure S6C), making EGFR-EDV-682 an ideal formulation for treatment.

P1 tolerated EGFR-EDV-682 well and reported a dramatic increase in well-being throughout treatment. The Eastern Cooperative Oncology Group performance status fell from 2 to 0 during that time. A transient rise in TNF-α and IL-6 at 3 h post dose, highest post dose 1 and lower in subsequent doses, was observed (Figure S6D). There were no changes in hematological and biochemistry parameters, and white cell count remained normal throughout the treatment. CA19-9 levels fell to 5,310 kU/L, and CRP levels fell to 7 mg/L at dose 12 (Figures 7A and S6E).

The second case is the use of EGFR-EDV-Dox in a patient with recurrent glioblastoma (P2). After one cycle, MRI showed marked shrinkage of primary tumor and stabilization in other sites. In addition, the patient reported improvement in quality of life specifically noting the ability to walk independently without a walking aid.

Immunophenotyping of major immune cell subsets from peripheral blood mononuclear cells revealed changes within multiple cell types that may support a favorable antitumor response. For P1, total $CD14^+$ monocytes, precursors for MΦs and DCs, increased by 105% at D12 as compared with the screen dose (D1) (Figure 7B), including the intermediate ($CD14^+CD16^{++}$) monocyte subset (69% increase; Figure 7C). Intermediate monocytes demonstrate the highest capacity to present antigen to T cells, with superior antigen-specific induction of IL-12 and IFN-γ (Ziegler-Heitbrock and Hofer, 2013). For P2, a $CD56^{dim}$ cytotoxic sub pool of NK cells exhibited a 55% increase at D7 compared with D1 (Figure 7D). Furthermore, cytotoxic natural killer T (NKT) cells increased (39%; Figure 7E), as did the rare invariant NKT sub pool which doubled (Figure 7F).

A 28% increase in myeloid DC (mDC) and a 60% decrease in plasmacytoid DC (pDC) were also observed in P1 (Figure 7G). A similar result for pDC was observed in P2, while the mDC remained unchanged (Figure S6F). In both patients, the antigen-presenting $Clec9A^+$ mDC, which are responsible for driving a $CD8^+$ effector T cell response, increased in circulation (P1, 98%; P2, 48%; Figure 7H). This increase was in concordance with increases in the total cytotoxic $CD8^+$ T cells (P1, 60%; P2,

(B) Interstitial cytokine concentration of IFN-α (a) IL-12p40 (b), and IFN-γ (c) in non-depleted and immune cell-depleted CT26Ep12.1 tumors (n = 4).
(C) Interstitial IL-2, IL-4, and IL-6 in CT26Ep12.1 tumors treated with saline (–) and Ep-EDV-682 (+) (n = 4). Data represent mean ± SEM and analyzed by two-way ANOVA and Tukey's multiple comparison test.
(D and E) Long-term survival of mice bearing 4T1 tumors (D) and CT26Ep12.1 tumors (E) treated with saline, Ep-EDV, and Ep-EDV-682 (n = 10 saline, Ep-EDV, n = 20 Ep-EDV-682). Red arrow, tumor re-challenge; green arrows, treatment. Kaplan-Meier test used for analysis.
(F and G) $CD8^+$ and $CD4^+$ memory T cell populations in 4T1 (F) and CT26Ep12.1 (G) tumors treated with saline or Ep-EDV-682. Data represent mean ± SEM and analyzed by two-way ANOVA and Tukey's multiple comparison test. *$p \leq 0.05$, **$p \leq 0.01$, ***$p \leq 0.001$, ****$p \leq 0.0001$.
See Figure S5.

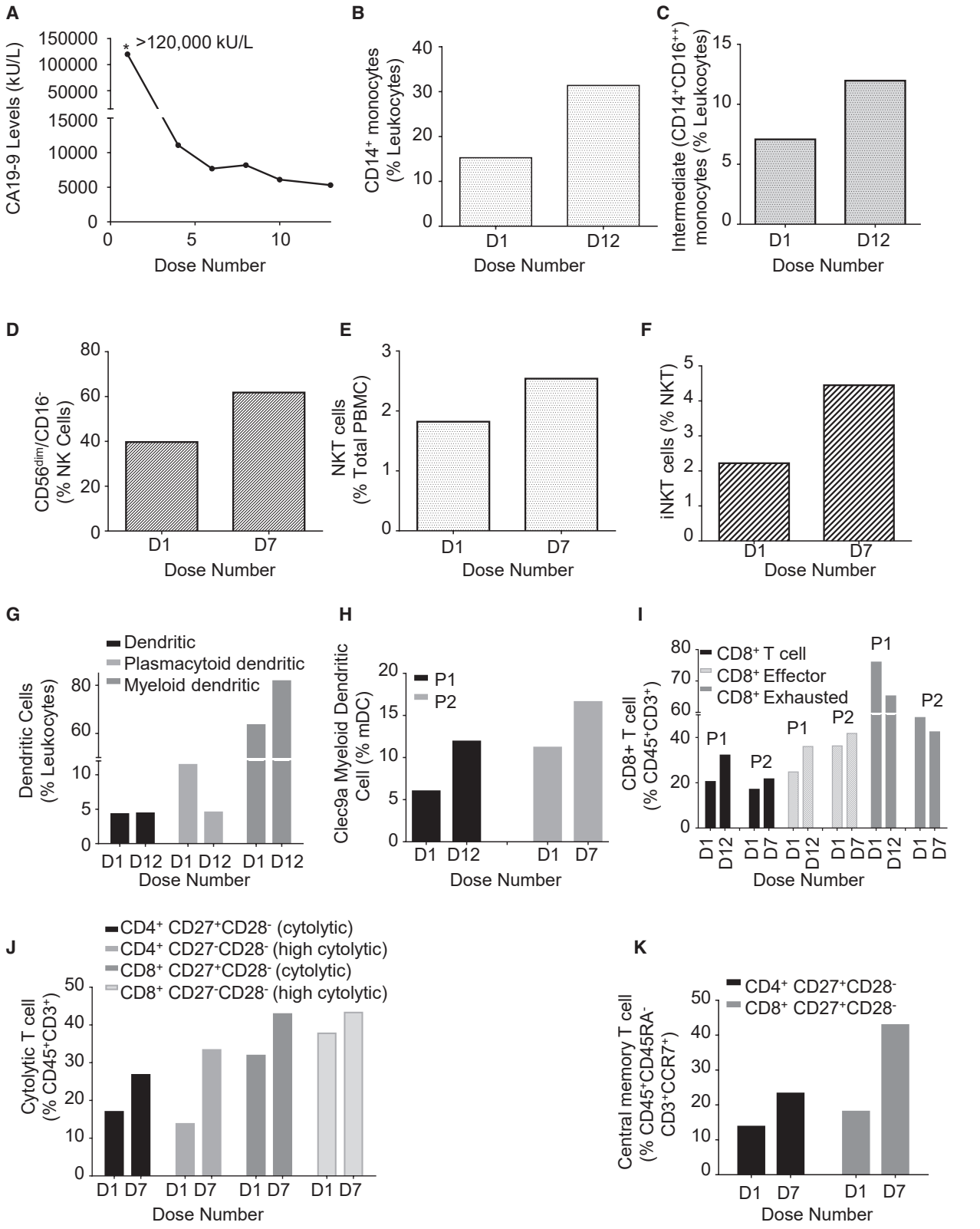

(legend on next page)

27%), including effector CD8$^+$ T cells (P1, 50%; P2, 15%) at D12 and D7, respectively (Figure 7I). Cytotoxic CD8$^+$ T cells expressing exhausted programmed death-1 (PD-1$^+$), indicative of prolonged cell activation and susceptibility to PD-1 ligation by tumor cells expressing PD-L1, decreased by 17% in P1 and 13% in P2 at D12 and D7, respectively. A similar decrease in exhausted CD4$^+$ T cells was observed in P2 (Figure S6G). Subtypes of CD8$^+$ cytotoxic T cells and CD4$^+$ T helper cells that contain the greatest amounts of cytolytic enzymes (Perforin, Granzyme A and B) increased in P2 (Figure 7J), with the greatest increase in the CD8$^+$ central memory pool (Figure 7K). In addition to data reported above, we have also seen favorable immune profiles in three patients after treatment with EGFR-targeted EDVs carrying mitoxantrone with increases in relevant DC, NK, and T cell populations after treatment (unpublished data). The results observed in these case studies follow a similar trend to those observed in the preclinical mouse models.

DISCUSSION

We have demonstrated the ability of targeted EDVs loaded with super-cytotoxin 682 to not only effectively deliver this drug to the tumor cells, but also elicit an immunotherapeutic antitumor immune response. Ep-EDV-682 treatment can activate immune cell subsets, including DCs, MΦ, NK, and CD8$^+$ T cells toward an antitumor phenotype capable of effectively eliminating tumor cells. When combined with the effectiveness of the drug, this results in a dual assault on the tumor which can confer not only long-term survival, but also resistance to tumor relapse.

The EDV represents a cyto-IMT which creates an immunogenic TME via the delivery of cytotoxic agents directly to the tumor, where it first stimulates the innate immune system toward an antitumor phenotype. An adaptive response in then triggered with tumor-specific cytotoxic T cells arising (Figure 8). Following intravenous administration, EDVs extravasate to the tumor where $\geq$30% of the administered dose is delivered directly into the TME within 2 h (MacDiarmid et al., 2007b). They then bind to surface receptors delivering their payload directly to the tumor cells. 682 delivery to tumor cells results in rapid apoptosis (Figure 8A). DAMP signals produced by apoptotic cells then interact with TAMs and stimulate upregulation of CD86 and production of Th1 pro-inflammatory cytokines, such as TNF-α and IL-6 (Figure 8B). These changes are typical in antitumor M1 MΦs, which are capable of killing tumor cells and releasing cytokines as activation signals for other immune cells (Sawa-Wejksza and Kandefer-Szerszen, 2018). The EDV itself can also directly polarize M1 TAMs via the LPS/TLR4 mechanism, thus further contributing to the initiation of an inflammatory antitumor environment, although the contribution from this interaction would be small (Zhou et al., 2018).

TAMs are generally the most abundant immune cells in the TME. Following Ep-EDV-682 treatment, TAMs made up 55% of infiltrating immune cells in CT26Ep12.1 tumors. The loss of Ep-EDV-682 efficacy with CD11b$^+$ depletion combined with a complete intolerance to EDV treatment after specific MΦ depletion points toward the importance of myeloid-derived cells, particularly MΦ, in facilitating the follow-on effects of an EDV-induced antitumor immune response.

Innate immune cells are some of the first to interact with EDVs either directly or through EDV-induced tumor cell apoptosis. Post-EDV interaction, TAMs secrete chemokines, which attract additional immune cells, such as NK cells, T cells, MΦs, and DCs (Allen et al., 2018), to the TME (Figure 8C). DCs are also capable of producing chemokines, with mDC shown to produce CCL2 in response to LPS stimulation and pDC shown to produce CCL3 in response to CpG stimulation (Penna et al., 2002). Ep-EDV-682 treatment significantly increased the local concentration of CCL2, CCL3, and CCL5 within the TME, while *in vivo* depletion of CD11b$^+$ cells resulted in a decrease in all three chemokines with a further decrease in CCL3 and CCL5 after Ep-EDV-682 treatment. The decrease in chemokine production translated to a decrease in infiltrating immune cell numbers in the TME, with a decrease in the proportion of NK and T cells.

DCs have been explored as a potential target in cancer immunotherapies as they are known to be the most effective APC and constitute the bridge between the innate and adaptive immune system (Anguille et al., 2015; Farkona et al., 2016). Current strategies for DC-based IMT involve *ex vivo* manipulation and priming of DC/DC precursors; however, success from this strategy has been limited (Anguille et al., 2015; Jung et al., 2018). EDV treatment allows for *in vivo* priming and maturation of DCs within the TME in response to dying tumor cells (Figure 8D). Immature DCs are capable of engulfing DAMPs and/or apoptotic tumor cell bodies within the TME. The engulfed molecules are then processed for antigen presentation on the DC surface via MHC class I and II molecules with concomitant DC maturation as indicated by upregulation of the costimulatory molecules CD86, CD80, and MHC class II. DC then migrate to draining lymph nodes for antigen presentation to T cells thereby increasing production of CD4$^+$ T helper cells and tumor-specific CD8$^+$ CTL and initiating an adaptive immune response to the tumor (Figure 8E). An increase in the production of Th1 cytokines, including type 1 IFNs, by DC co-cultured with Ep-EDV-682-treated tumor cells and within the TME after Ep-EDV-682 treatment was observed and is known to be associated with favorable disease outcomes (Cauwels et al., 2018; Fitzgerald-Bocarsly and Feng, 2007; Zitvogel et al., 2015). CD11b$^+$ cell depletion experiments showed a significant decrease in the local tumor IFN-α concentration with a further decrease after Ep-EDV-682 treatment. A similar

Figure 7. Patient Response to Drug-Loaded EGFR-Targeted EDVs

(A) CA19-9 serum levels in patient P1 on a clinical trial at different time points after treatment with EGFR-EDV-682.

(B–K) Duraclone immunophenotyping of PBMC from patients on clinical trials being treated with EGFR-EDV-682 (P1) or EGFR-EDV-Dox (P2) at the indicated dose number: P1 monocytes (CD14$^+$) (B); P1 antigen-presenting monocytes (CD14$^+$CD16^{++}) as a percentage of leukocytes (C); P2 CD56^{dim} cytotoxic NK cell sub pool, as a percentage of total NK cells (D); P2 NKT cell sub pool, as a percentage of total PBMC (E); P2 invariant NKT sub pool, as a percentage of total NKT cells (F); P1 DC subtypes as a percentage of leukocytes (G); P1 and P2 myeloid dendritic cells (Clec9A$^+$) as a percentage of mDC (H); P1 and P2 CD8$^+$ T cell subtypes (I); P2 CD4$^+$ and CD8$^+$ cytolytic T cell subtypes (J); P2 central memory populations (K).

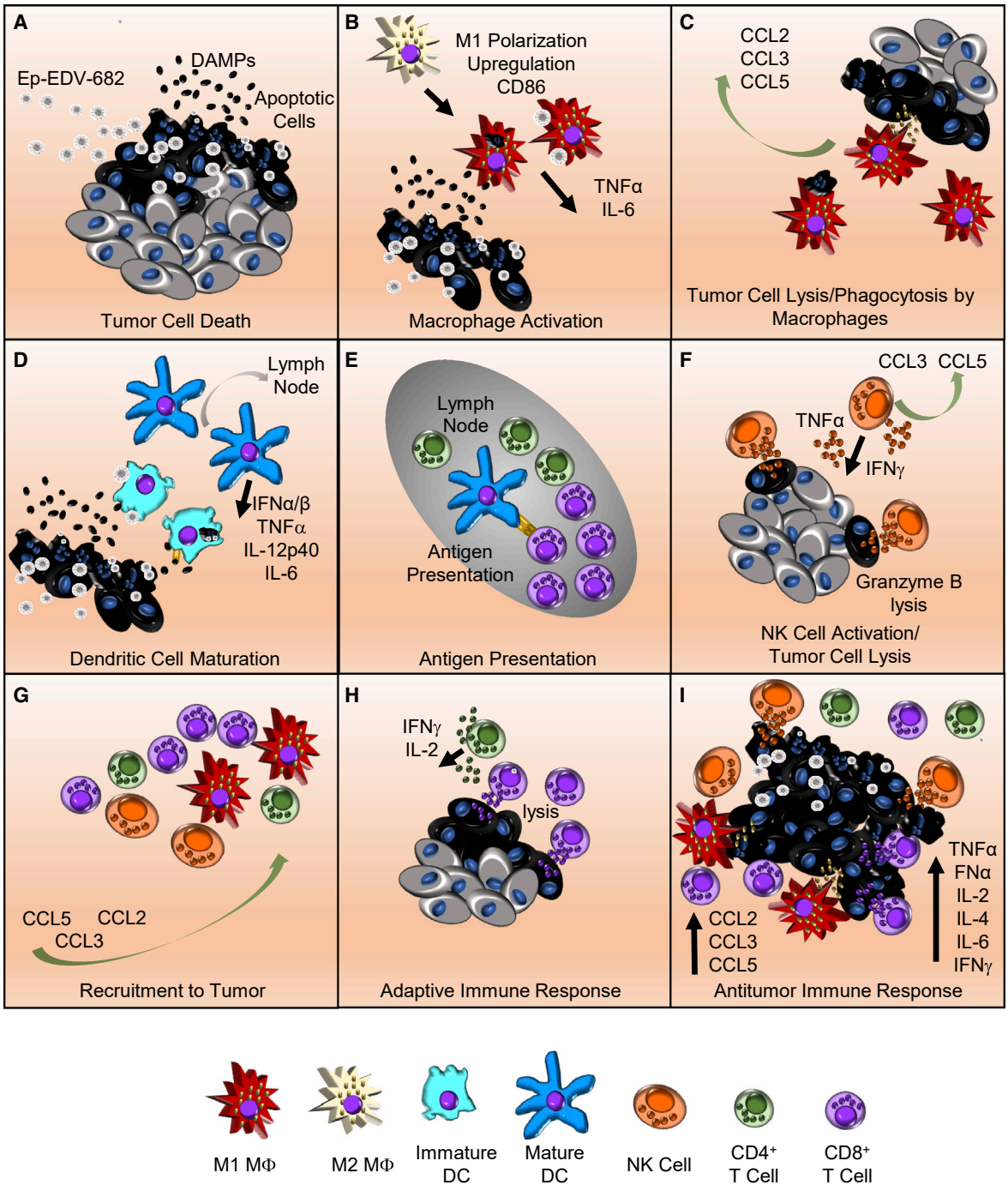

Figure 8. Schematic of the Proposed Mechanism of EDV-Induced Activation of the Immune System

(A) Ep-EDV-682 enters the TME via the leaky vasculature resulting in tumor cell apoptosis and the release of immune-activating DAMPs.

(B and C) MΦs within the TME engulf apoptotic cells or interact directly with EDVs resulting in M1 MΦ polarization and release of inflammatory cytokines (B); M1 MΦs lyse tumor cells and release chemokines (C).

(D) Immature DCs engulf apoptotic cell bodies and tumor antigens released in response to Ep-EDV-682 treatment and mature releasing type 1 interferons, TNF-α, IL-12p40, and IL-6.

(E) Mature DCs migrate to lymph nodes for antigen presentation to T cells.

(F) NK cell activation occurs in the TME resulting in release of IFN-γ, IL-2, and TNF-α as well as chemokines. Activated NK cells also effectively lyse tumor cells.

(G and H) Release of chemokines recruits additional T cells, NK cells, and MΦs into the TME (G). Tumor-specific $CD8^+$ T cells then contribute the response via tumor cell lysis (H).

(I) All of these steps combine to create an effective antitumor immune response.

trend was observed with IL-12p40, which promotes Th1 differentiation of T cells and is primarily produced by MΦs, DC, and NK cells, indicating that myeloid-derived cells are major contributors of IFN-α and IL-12p40 production after Ep-EDV-682 treatment *in vivo*.

EDV treatment is also capable of eliciting NK cell activation leading to increased cytotoxicity (Figure 8F). NK cells possess the inherent ability to lyse malignant cells in an antigen-independent manner. IL-2, IFN-γ, and IFN-α, which are significantly increased in the TME of Ep-EDV-682-treated tumors, are known to activate NK cells toward both increased cytokine production and enhanced cytolytic function (Fang et al., 2017; Lee and Margolin, 2011; Morvan and Lanier, 2016). Immature, intermediate, and mature mouse NK cells express CCR1, CCR2, and CCR5 chemokine receptors that can bind the chemokines CCL2, CCL3, and CCL5, all of which are upregulated in Ep-EDV-682-treated tumors as well as by MΦs and NK cells from Ep-EDV-682-treated mice. These results highlight the important contribution of NK cells to enhanced cytolytic efficacy, as well as the production of chemokines and cytokines vital for recruitment and activation of additional immune cells after Ep-EDV-682 treatment.

EDV treatment subsequently induces an adaptive immune response in which tumor-specific CTLs and T helper cells are produced and then recruited to the tumor site (Figure 8G). As with innate cells, CCL2, CCL3, and CCL5 play a large role in recruitment of T cells to the TME, while IFN-γ, IL-12, and TNF-α are vital for generating Th1 effector cells (Allen et al., 2018; Brown et al., 2007). Following recruitment, tumor-specific CTLs target and lyse tumor cells (Figure 8H). Nude mice, which lack T cells, responded effectively to Ep-EDV-682 treatment, suggesting a minimal role for the adaptive response in overall efficacy. However, this was far from the case in immunocompetent animals. Differences observed between human xenografts in nude mice as compared with syngeneic models in immunocompetent mice are difficult to draw comparisons from as tumor growth and response to treatment is distinct for each model. Specific depletion of T cells from the immunocompetent CT26Ep12.1 model allowed for a more direct comparison, as well as observation of the specific roles of $CD4^+$ and $CD8^+$ T cells in Ep-EDV-682 efficacy. Despite slowing tumor growth, $CD4^+$ T cell depletion did not enhance Ep-EDV-682 efficacy. Furthermore, $CD4^+$ T cell response to EDV treatment was vital in promoting MΦ infiltration. In contrast, $CD8^+$ T cell depletion resulted in reduced Ep-EDV-682 efficacy, notable after 1 week, which corresponds to the time required for mounting an adaptive immune response. Increases in NK cell infiltration in response to Ep-EDV-682 treatment was reliant on $CD8^+$ T cells, while MΦ and $CD4^+$ T cell infiltration as well as cytokine/chemokine production were not.

Combined, the results support differential roles for a variety of immune cell subsets in their contribution to the efficacy of targeted, drug-loaded EDVs in solid tumors. Furthermore, targeted, drug-loaded EDV treatment elicits a predominantly Th1 response as demonstrated by the increase of Th1 cytokines (TNF-α, IFN-α, IFN-γ, IL-2, and IL-6) within the TME. Although an increase in IL-4, a cytokine generally identified as Th2, was also observed in the 4T1 model, it is important to note the pleiotropic nature of most cytokines (Carvalho et al., 2002). Therefore, future studies will be necessary to fully deduce the role of individual cytokines as it pertains to EDV-induced immune cell activation.

As with innate cells, T cells are also capable of producing cytokines, which in addition to promoting cytolytic function are responsible for driving the production of Th1 $CD4^+$ T cells (Belardelli and Ferrantini, 2002; Lee and Margolin, 2011). Release of Th1 cytokines by either innate immune cells or T cells are responsible for co-stimulation, activation, growth, and increased antigen presentation, creating a feedback loop which further enhances the antitumor activity of the immune system (Figure 8I). It is important to note that data obtained here is a snapshot of the TME after repeated EDV administration, and only provides a basic mechanistic understanding of EDV-induced antitumor immunity. Furthermore, the focus herein has been only on major immune cell subsets; however, small, specific subpopulations can have large overall effects. These considerations are beyond the scope of the current study; however, future studies will begin to deconvolute EDV-induced antitumor immunity by addressing these issues more specifically.

EDVs possess advantages over current IMT strategies in that immune cell activation occurs both *in vivo* and primarily at the tumor site, which is a rapidly changing, dynamic environment. It creates an immunogenic tumor environment and elicits effects on multiple arms of the immune system, thereby avoiding problems associated with patients who show little to no immune response to their tumors or adaptations to therapies which only target single immune cell populations. The current study highlights the potential of the EDV as a cancer IMT, and future EDV formulations could exploit its inherent immunogenic nature given the versatility of this technology with respect to both payload and targeting ability.

STAR★METHODS

Detailed methods are provided in the online version of this paper and include the following:

- KEY RESOURCES TABLE
- LEAD CONTACT AND MATERIALS AVAILABILITY
- EXPERIMENTAL MODEL AND SUBJECT DETAILS
  - Clinical Trial ACTRN12617000037303
  - Clinical Trial
  - *In Vivo* Tumor Models
- METHOD DETAILS
  - EnGeneIC Dream Vector (EDV)
  - Flow Cytometry
  - Cell Culture
  - Bone Marrow Derived DCs (BMDC)
  - Treatment of RAW264.7 Cells with EDVs
  - Macrophage and DC/Tumor Cell Co-cultures
  - In Vivo Immune Cell Depletion
  - Isolation of $CD11b^+$ Cells from 4T1 and CT26Ep12.1 Tumor
  - Isolation of NK and CD8 from Spleens
  - xCELLigence Monitored $CD11b^+$, $CD8^+$, and NK Cell Cytolysis of Tumor Cells
  - NK Cell Mediated Cytolysis Inhibition
  - Tumor/Spleen Flow Cytometry
  - Cytokine and Chemokine Detection

SUPPLEMENTAL INFORMATION

Supplemental Information can be found online at https://doi.org/10.1016/j.ccell.2020.02.001.

ACKNOWLEDGMENTS

All research was funded by EnGeneIC Ltd.

AUTHOR CONTRIBUTIONS

Conceptualization, S.M.S., J.A.M., and H.B.; Methodology, S.M.S., J.A.M., and H.B.; Formal Analysis, S.M.S.; Investigation, S.M.S., L.Y., E.M.E., E.B., K.S., S.L.P., G.E.S., E.S.C., and N.V.; Resources, J.B. and S.C.; Writing – Original Draft, S.M.S.; Writing – Review & Editing, S.M.S., J.A.M., H.B., and S.L.P.; Visualization, S.M.S.; Supervision, S.M.S., J.A.M., and H.B.; Funding Acquisition, J.A.M. and H.B.

DECLARATION OF INTERESTS

H.B. and J.A.M. have ownership interests (including patents) in EnGeneIC Ltd. S.M.S., L.Y., E.M.E., K.S., N.V., S.L.P., and E.S. are employees of EnGeneIC Ltd. The other authors declare no conflict of interest.

Received: September 13, 2018
Revised: August 8, 2019
Accepted: February 4, 2020
Published: March 16, 2020

REFERENCES

Allen, F., Bobanga, I.D., Rauhe, P., Barkauskas, D., Teich, N., Tong, C., Myers, J., and Huang, A.Y. (2018). CCL3 augments tumor rejection and enhances CD8(+) T cell infiltration through NK and CD103(+) dendritic cell recruitment via IFNgamma. Oncoimmunology *7*, e1393598.

Anguille, S., Smits, E.L., Bryant, C., Van Acker, H.H., Goossens, H., Lion, E., Fromm, P.D., Hart, D.N., Van Tendeloo, V.F., et al. (2015). Dendritic cells as pharmacological tools for cancer immunotherapy. Pharmacol. Rev. *67*, 731–753.

Belardelli, F., and Ferrantini, M. (2002). Cytokines as a link between innate and adaptive antitumor immunity. Trends. Immunol. *23*, 201–208.

Brown, C.E., Vishwanath, R.P., Aguilar, B., Starr, R., Najbauer, J., Aboody, K.S., and Jensen, M.C. (2007). Tumor-derived chemokine MCP-1/CCL2 is sufficient for mediating tumor tropism of adoptively transferred T cells. J. Immunol. *179*, 3332–3341.

Carvalho, L.H., Sano, G.-i., Hafalla, J.C.R., Morrot, A., de Lafaille, M.A.C., and Zavala, F. (2002). IL-4-secreting CD4+ T cells are crucial to the development of CD8+ T-cell responses against malaria liver stages. Nat. Med. *8*, 166–170.

Cauwels, A., Van Lint, S., Paul, F., Garcin, G., De Koker, S., Van Parys, A., Wueest, T., Gerlo, S., Van der Heyden, J., Bordat, Y., et al. (2018). Delivering type I interferon to dendritic cells empowers tumor eradication and immune combination treatments. Cancer Res. *78*, 463–474.

D'Aloia, M.M., Zizzari, I.G., Sacchetti, B., Pierelli, L., and Alimandi, M. (2018). CAR-T cells: the long and winding road to solid tumors. Cell Death Dis. *9*, 282.

Dong, P., Ma, L., Liu, L., Zhao, G., Zhang, S., Dong, L., Xue, R., and Chen, S. (2016). CD86(+)/CD206(+), diametrically polarized tumor-associated macrophages, predict hepatocellular carcinoma patient prognosis. Int. J. Mol. Sci. *17*, 320.

Dudek, A.M., Martin, S., Garg, A.D., and Agostinis, P. (2013). Immature, semi-mature, and fully mature dendritic cells: toward a DC-cancer cells interface that augments anticancer immunity. Front. Immunol. *4*, 438.

Emens, L.A., Ascierto, P.A., Darcy, P.K., Demaria, S., Eggermont, A.M.M., Redmond, W.L., Seliger, B., and Marincola, F.M. (2017). Cancer immunotherapy: opportunities and challenges in the rapidly evolving clinical landscape. Eur. J. Cancer *81*, 116–129.

Fang, F., Xiao, W., and Tian, Z. (2017). NK cell-based immunotherapy for cancer. Semin. Immunol. *31*, 37–54.

Farkona, S., Diamandis, E.P., and Blasutig, I.M. (2016). Cancer immunotherapy: the beginning of the end of cancer? BMC Med. *14*, 73.

Fitzgerald-Bocarsly, P., and Feng, D. (2007). The role of type I interferon production by dendritic cells in host defense. Biochimie *89*, 843–855.

Jenkins, R.W., Barbie, D.A., and Flaherty, K.T. (2018). Mechanisms of resistance to immune checkpoint inhibitors. Br. J. Cancer *118*, 9–16.

Jung, N.C., Lee, J.H., Chung, K.H., Kwak, Y.S., and Lim, D.S. (2018). Dendritic cell-based immunotherapy for solid tumors. Transl. Oncol. *11*, 686–690.

Kao, S.C., Fulham, M., Wong, K., Cooper, W., Brahmbhatt, H., MacDiarmid, J.A., Pattison, S.T., Sagong, J.O., Huynh, Y., Leslie, F., et al. (2015). A significant metabolic and radiological response following a novel targeted microRNA-based treatment approach in malignant pleural mesothelioma. Am. J. Respir. Crit. Care Med. *191*, 1467–1469.

Lanca, T., Costa, M.F., Goncalves-Sousa, N., Rei, M., Grosso, A.R., Penido, C., and Silva-Santos, B. (2013). Protective role of the inflammatory CCR2/CCL2 chemokine pathway through recruitment of type 1 cytotoxic gamma-delta T lymphocytes to tumor beds. J. Immunol. *190*, 6673–6680.

Lee, S., and Margolin, K. (2011). Cytokines in cancer immunotherapy. Cancers *3*, 3856–3893.

MacDiarmid, J.A., Amaro-Mugridge, N.B., Madrid-Weiss, J., Sedliarou, I., Wetzel, S., Kochar, K., Brahmbhatt, V.N., Phillips, L., Pattison, S.T., Petti, C., et al. (2009). Sequential treatment of drug-resistant tumors with targeted minicells containing siRNA or a cytotoxic drug. Nat. Biotechnol. *27*, 643–651.

MacDiarmid, J.A., Madrid-Weiss, J., Amaro-Mugridge, N.B., Phillips, L., and Brahmbhatt, H. (2007a). Bacterially-derived nanocells for tumor-targeted delivery of chemotherapeutics and cell cycle inhibitors. Cell Cycle *6*, 2099–2105.

MacDiarmid, J.A., Mugridge, N.B., Weiss, J.C., Phillips, L., Burn, A.L., Paulin, R.P., Haasdyk, J.E., Dickson, K.A., Brahmbhatt, V.N., Pattison, S.T., et al. (2007b). Bacterially derived 400 nm particles for encapsulation and cancer cell targeting of chemotherapeutics. Cancer Cell *11*, 431–445.

Mellman, I., Coukos, G., and Dranoff, G. (2011). Cancer immunotherapy comes of age. Nature *480*, 480–489.

Morvan, M.G., and Lanier, L.L. (2016). NK cells and cancer: you can teach innate cells new tricks. Nat. Rev. Cancer *16*, 7–19.

Oiseth, S.J., and Aziz, M.S. (2017). Cancer immunotherapy: a brief review of the history, possibilities, and challenges ahead. J. Cancer Metastasis Treat. *3*, 250.

Penna, G., Vulcano, M., Roncari, A., Facchetti, F., Sozzani, S., and Adorini, L. (2002). Cutting edge: differential chemokine production by myeloid and plasmacytoid dendritic cells. J. Immunol. *169*, 6673–6676.

Quintieri, L., Geroni, C., Fantin, M., Battaglia, R., Rosato, A., Speed, W., Zanovello, P., and Floreani, M. (2005). Formation and antitumor activity of PNU-159682, a major metabolite of nemorubicin in human liver microsomes. Clin. Cancer Res. *11*, 1608–1617.

Sabry, M., and Lowdell, M.W. (2013). Tumor-primed NK cells: waiting for the green light. Front. Immunol. *4*, 408.

Sagnella, S.M., Trieu, J., Brahmbhatt, H., MacDiarmid, J.A., MacMillan, A., Whan, R.M., Fife, C.M., McCarroll, J.A., Gifford, A.J., Ziegler, D.S., and Kavallaris, M. (2018). Targeted doxorubicin-loaded bacterially derived nanocells for the treatment of neuroblastoma. Mol. Cancer Ther. *17*, 1012–1023.

Sawa-Wejksza, K., and Kandefer-Szerszen, M. (2018). Tumor-associated macrophages as target for antitumor therapy. Arch. Immunol. Ther. Exp. *66*, 97–111.

Sharma, P., Hu-Lieskovan, S., Wargo, J.A., and Ribas, A. (2017). Primary, adaptive, and acquired resistance to cancer immunotherapy. Cell *168*, 707–723.

Sharpe, A.H. (2017). Introduction to checkpoint inhibitors and cancer immunotherapy. Immunol. Rev. *276*, 5–8.

Simmons, D.P., Wearsch, P.A., Canaday, D.H., Meyerson, H.J., Liu, Y.C., Wang, Y., Boom, W.H., and Harding, C.V. (2012). Type I IFN drives a distinctive dendritic cell maturation phenotype that allows continued class II MHC synthesis and antigen processing. J. Immunol. *188*, 3116–3126.

Solomon, B.J., Desai, J., Rosenthal, M.A., McArthur, G.A., Pattison, S.T., Pattison, S.L., MacDiarmid, J.A., Brahmbhatt, H., and Scott, A.M. (2015). A first-time-in-human phase I clinical trial of bispecific antibody-targeted, paclitaxel-packaged bacterial minicells. PLoS One *10*, 1–17.

Staudacher, A.H., and Brown, M.P. (2017). Antibody drug conjugates and bystander killing: is antigen-dependent internalisation required? Br. J. Cancer *117*, 1736–1742.

Szkandera, J., Stotz, M., Absenger, G., Stojakovic, T., Samonigg, H., Kornprat, P., Schaberl-Moser, R., Alzoughbi, W., Lackner, C., Ress, A.L., et al. (2014). Validation of C-reactive protein levels as a prognostic indicator for survival in a large cohort of pancreatic cancer patients. Br. J. Cancer *110*, 183–188.

van Zandwijk, N., Pavlakis, N., Kao, S.C., Linton, A., Boyer, M.J., Clarke, S., Huynh, Y., Chrzanowska, A., Fulham, M.J., Bailey, D.L., et al. (2017). Safety and activity of microRNA-loaded minicells in patients with recurrent malignant pleural mesothelioma: a first-in-man, phase 1, open-label, dose-escalation study. Lancet Oncol. *18*, 1386–1396.

Ventola, C.L. (2017). Cancer immunotherapy, part 2: efficacy, safety, and other clinical considerations. Pharm. Ther. *42*, 452–463.

Whittle, J.R., Lickliter, J.D., Gan, H.K., Scott, A.M., Simes, J., Solomon, B.J., MacDiarmid, J.A., Brahmbhatt, H., and Rosenthal, M.A. (2015). First in human nanotechnology doxorubicin delivery system to target epidermal growth factor receptors in recurrent glioblastoma. J. Clin. Neurosci. *22*, 1889–1894.

Yuan, A., Hsiao, Y.J., Chen, H.Y., Chen, H.W., Ho, C.C., Chen, Y.Y., Liu, Y.C., Hong, T.H., Yu, S.L., Chen, J.J., and Yang, P.C. (2015). Opposite effects of M1 and M2 macrophage subtypes on lung cancer progression. Sci. Rep. *5*, 14273.

Zhou, S., Gravekamp, C., Bermudes, D., and Liu, K. (2018). Tumour-targeting bacteria engineered to fight cancer. Nat. Rev. Cancer *18*, 727–743.

Ziegler-Heitbrock, L., and Hofer, T.P. (2013). Toward a refined definition of monocyte subsets. Front. Immunol. *4*, 23.

Zitvogel, L., Galluzzi, L., Kepp, O., Smyth, M.J., and Kroemer, G. (2015). Type I interferons in anticancer immunity. Nat. Rev. Immunol. *15*, 405–414.

STAR★METHODS

KEY RESOURCES TABLE

REAGENT or RESOURCE	SOURCE	IDENTIFIER
Antibodies		
Duraclone IM T Cell Subsets tube	Beckman Coulter	B53328
Duraclone IM Dendritic Cell tube	Beckman Coulter	B53351
Duraclone IM Th1/Th2 Cell tube	Beckman Coulter	B74674
Duraclone IM Count tube	Beckman Coulter	C00162
Duraclone IM Treg tube	Beckman Coulter	B53346
Duraclone Custom Basic tube	Beckman Coulter	This paper
Duraclone Custom iNKT tube	Beckman Coulter	This paper
Anti-Human TCRvbeta11-FITC ASR	Beckman Coulter	IM1586; RRID: AB_131027
Anti- Human TCR VAlpha-PE	Beckman Coulter	IM2283; RRID: AB_131321
Anti- Human CD69 PE/Dazzle	BioLegend	310941; RRID: AB_2564276
Anti- Human CD56 PE/Cy7	BioLegend	362509; RRID: AB_2563926
Anti- Human CXCR3	BioLegend	353709; RRID: AB_10962570
Anti- Human CD28	BioLegend	302941; RRID: AB_2564234
Anti- Human CCR4	BioLegend	359409; RRID: AB_2562430
Anti- Human CD45RA	BioLegend	304129; RRID: AB_10900421
Anti- Human CD16 FITC	BioLegend	302005; RRID: AB_314205
Anti- Human CD19 PE/Dazzle 594	BioLegend	302251; RRID: AB_2563559
Anti- Human CD86 PE/Cy5	BioLegend	305407; RRID: AB_314527
Anti- Human CD14 PE/Cy7	BioLegend	301813; RRID: AB_389352
Anti- Human CD206 BV421	BioLegend	321126; RRID: AB_2563839
APC anti-mouse CD326 (Ep-CAM) Antibody	BioLegend	118214; RRID: AB_1134102
Anti-Rae-1α/β/γ-PE, mouse	Miltenyi	130-109-011; RRID: AB_2653332
Anti-H60a-PE, mouse	Miltenyi	130-108-820; RRID: AB_2651974
Mouse ULBP-1/MULT-1 PE-conjugated Antibody	R&D Systems	FAB2588P; RRID: AB_10973344
Mouse Rae-1 alpha / beta / gamma Antibody	R&D Systems	MAB1758; RRID: AB_2253397
Mouse H60 Antibody	R&D Systems	MAB1155; RRID: AB_2115297
DAPI	Life Technologies	D1306; RRID: AB_2629482
APC anti-mouse CD326	Biolegend	118214; RRID: AB_1134102
Brilliant Violet 510™ anti-mouse CD45 Antibody	Biolegend	103138; RRID: AB_2563061
Anti-mouse CD45 PE/Cy5	Biolegend	103110; RRID: AB_312975
anti-CD45 PECy7	Biolegend	103114; RRID: AB_312979
APC/Cy7 anti-mouse CD86 Antibody	Biolegend	105030; RRID: AB_2244452
anti-CD45 APC/Fire750	Biolegend	103154; RRID: AB_2572116
Mouse MMR/CD206 Alexa Fluor® 488-conjugated Antibody	R&D Systems	FAB2535G; RRID: AB_10971285
Anti-CD11b antibody [M1/70] (Alexa Fluor 488)	Abcam	ab197701
CD11c Monoclonal Antibody (N418), PE	Molecular Probes	MCD11c04; RRID: AB_10372340
MHC Class II (I-A/I-E) Monoclonal Antibody (M5/114.15.2), PE-Cyanine5	eBioscience (Thermofisher)	15-5321-82; RRID: AB_468800
MHC Class II Brilliant Violet 421	Biolegend	107631; RRID: AB_10900075
7-AAD	Biolegend	420404
CD80 PE	eBioscience (Thermofisher)	12-0801-82; RRID: AB_465752
APC anti-mouse CD11b	BioLegend	101212;RRID: AB_312795
anti-CD3e APC-eFluor780	eBioscience	47-0031-82; RRID: AB_11149861
anti-CD3 APC	Molecular Probes: Life Technologies	A18605; RRID: AB_2535395

(*Continued on next page*)

Continued

REAGENT or RESOURCE	SOURCE	IDENTIFIER
anti-CD4 PE-TR	Abcam	ab51467; RRID: AB_868922
anti-CD4 PE-TR (RM4-5)	Molecular Probes: Life Technologies	MCD0417; RRID: AB_1474397
anti-CD8a FITC	eBioscience	11-0081-82; RRID: AB_464915
anti-CD8 BV510	BioLegend	100751;RRID: AB_2561389
anti-CD8b FITC	BioLegend	126606; RRID: AB_961295
anti-CD25 PE	Abcam	ab24933; RRID: AB_470364
anti-CD314 (NKG2D) PE-eFluor610	eBioscience	61-5882-82; RRID: AB_2574628
anti-CD335 (NKp46) PECy7	BioLegend	137618; RRID: AB_11219186
anti-CD27 BV421	BioLegend	124223; RRID: AB_2565547
ant-CD183 (CXCR3) BV510	BioLegend	126527; RRID: AB_2562204
anti-NKG2A/C/E FITC	eBioscience	11-5896-82; RRID: AB_465305
anti-CD11b APC	BD Pharmingen	553312; RRID: AB_398535
anti-CD11b APC (3A33)	Southern Biotech	1560-11; RRID: AB_2794902
anti-CD49b APC-eFluor780	eBioscience	47-5971-80; RRID: AB_11218495
anti-Ly6C FITC	BioLegend	128022; RRID: AB_10639728
anti-Ly6G BV510	BioLegend	127633; RRID: AB_2562937
anti-F4/80 PE Dazzle594	Biolegend	123146; RRID: AB_2564133
anti-CD206 PECy7	Biolegend	141720; RRID: AB_2562248
propidium iodide	sigma	P4864-10ML
DRAQ5	Thermo Fisher	62251
Live/Dead Yellow	Thermo Fisher	L34967
InVivoPlus anti-mouse CD4	BioXCell	BP0003-1; RRID: AB_1107636
InVivoPlus anti-mouse CD8α	BioXCell	BP0061; RRID: AB_1125541
InVivoMAb anti-mouse/human CD11b	BioXCell	BE0007; RRID: AB_1107582
Control Liposomes	Liposoma	C-010
Clodronate Liposomes	Liposoma	CP-005-005
Ultra-LEAF purified anti-Asialo-GM1	Biolegend	146002; RRID: AB_2562206
Biological Samples		
Patient PBMC	This Paper	N/A
Chemicals, Peptides, and Recombinant Proteins		
Red Blood Cell Lysing Buffer Hybri-Max	Sigma	R7757-100mL
3, 3′,5 ,5′-Tetramethylbenzidine Liquid Substrate	Merk	T0440
PerFix-nc kit	Beckman Coulter	B31167
IOTest 3 Fixative solution	Beckman Coulter	A07800
Lipofectamine® 2000 Transfection Reagent	Invitrogen	11668019
MTS Reagent Powder	Promega	G1112
Critical Commercial Assays		
NK Cell Isolation Kit, mouse	Miltenyi Biotec	130-115-818
$CD8a^+$ T Cell Isolation Kit, mouse	Miltenyi Biotec	130-104-075
CD11b microbeads, human and mouse	Miltenyi Biotec	130-049-601
Tumor Dissociation Kit, mouse	Miltenyi Biotec	130-096-730
RNAase plus mini kit	Qiagen	74134
Super Script VILO cDNA Synthesis Kit	Invitrogen	11754250
TaqMan® Fast Advanced Master Mix	Applied Biosystems™	4444557
Mouse IL-1beta DuoSet ELISA	R&D Systems	DY401
Mouse TNFalpha DuoSet ELISA	R&D Systems	DY410
Mouse IL-2 DuoSet ELISA	R&D Systems	DY402
Mouse IL-4 DuoSet ELISA	R&D Systems	DY404

(*Continued on next page*)

Continued

REAGENT or RESOURCE	SOURCE	IDENTIFIER
Mouse IL-6 DuoSet ELISA	R&D Systems	DY406
Mouse IL-12p40 DuoSet ELISA	R&D Systems	DY2398
Mouse IFNgamma DuoSet ELISA	R&D Systems	DY485
Mouse CCL2 DuoSet ELISA	R&D Systems	DY479
Mouse CCL3 DuoSet ELISA	R&D Systems	DY450
Mouse CCL5 DuoSet ELISA	R&D Systems	DY478
VeriKine Mouse IFN Alpha ELISA	PBL Assay Science	42120
Human IL-6 DuoSet ELISA	R&D Systems	DY206
Human TNFalpha DuoSet ELISA	R&D Systems	DY210
Quantum™ Simply Cellular® anti-Rat	Bangs Laboratories	817
PNU-159682	Levena Biopharma (Suzhou, China)	LN-T-5175
Gemcitabine	Sigma	G6423
Abraxane	Celgene	6200324
5-flouro-uracil	Sigma	F6256
Folinic Acid	Sigma	F7878
Oxaliplatin	Sigma	O9512
Irinotecan	Sigma	I1406
Experimental Models: Cell Lines		
4T1; murine breast cancer cell line	ATCC	ATCC CRL-2539; RRID: CVCL_0125
A549; human non-small cell lung cancer cell line	ECACC	86012804; RRID: CVCL_0023
A549DoxR; human non-small cell lung cancer cell line, multi-drug resistant	Made in house from parental A549 (ECACC)	N/A
CT26.WT; murine colon carcinoma cell line	ATCC	ATCC CRL-2638; RRID: CVCL_7256
CT26Ep12.1; murine colon carcinoma cell line, clone expressing EpCAM receptor	This paper	N/A
JAWSII; murine dendritic cell line	ATCC	ATCC CRL-11904; RRID: CVCL_3727
Patient Pancreatic Cells; cells derived from a human patient pancreatic tumour	This paper	N/A
RAW264.7; murine macrophage cell line	ATCC	ATCC T1B-71; RRID: CVCL_0493
T84; human colorectal carcinoma cell line	ECACC	88021101; RRID: CVCL_0555
Experimental Models: Organisms/Strains		
BALB/c	Animal Resource Centre	BALB/cArc
BALB/c Nude	Animal Resource Centre	BALB/c Fox1^{nu}/ARC
Oligonucleotides		
Taqman Gene Expression Assay-IFNa	Applied Biosystems	IFNa Mm03030145_gH
Taqman Gene Expression Assay-IFNb	Applied Biosystems	IFNb1 Mm00439552_s1
Taqman Gene Expression Assay-GAPDH	Applied Biosystems	GAPDH Mm99999915_g1
Recombinant DNA		
pcDNA3.1+/C-(K)DYK with mouse EpCAM ORF clone (NM_008532.2)	GenScript	Clone ID: OMu21996 https://www.genscript.com/gene/mus-musculus/17075/epcam.html
Software and Algorithms		
KC Junior version 1.4	BioTek Instruments	www.biotek.com
Kaluza Analysis version 2.1	Beckman Coulter	www.beckman.com
GraphPad Prism Ver 6.0	Prism	www.graphpad.com

LEAD CONTACT AND MATERIALS AVAILABILITY

Further information and requests for resources and reagents should be directed to and will be fulfilled by the Lead Contact, Dr Himanshu Brahmbhatt. (hbrahmbhatt@engeneic.com). All unique/stable reagents generated in this study are available from the Lead Contact with a completed Materials Transfer Agreement.

EXPERIMENTAL MODEL AND SUBJECT DETAILS

All participants in clinical trials signed a patient informed consent form prior to commencement of treatment.

Clinical Trial ACTRN12617000037303

Clinical Trial ACTRN12617000037303 is A Phase 1 Study of Anti-Human EGFR (Vectibix Sequence) Targeted EDVs Carrying the Cytotoxic Drug PNU-159682 (EGFR(V)-EDV-PNU) with Concurrent Non-Targeted EDVs Carrying an Immunomodulatory Adjuvant (EDV-40mer) in Subjects with Advanced Solid Tumours who have No Curative Treatment Options. A 67-year old Caucasian female, P1, whose primary symptom was jaundice, had previously undergone a complete Whipple procedure for pancreatic ductal adenocarcinoma (PDAC), to remove the pancreas, the gallbladder, the duodenum, the spleen and a portion of the stomach and surrounding lymph nodes. She had tumors in both the head and tail of the pancreas and her disease was diagnosed as Stage IV. Diagnostic evaluation of P1 included computerized axial tomography (CT) of the abdomen (May 2017) which revealed multiple low-density liver lesions. The tumors were not avid on positron emission tomography (PET). Serum levels of CA19-9, a carbohydrate antigen that is expressed on some gastrointestinal malignancies, particularly pancreatic cancers, and shown to be a prognostic indicator of overall survival and response to therapy, were assessed. Similarly, C-reactive protein (CRP) levels were also examined as elevated CRP levels is associated with poor clinical outcomes (Szkandera et al., 2014). She was treated with gemcitabine followed by FOLFIRINOX at another institution but had developed extensive metastatic disease in the liver on treatment. At the conclusion of her chemotherapy, sixteen months after her Whipple procedure, she had exhausted all treatment options, her weight was down from 62 kg to 45 kg, and she sought experimental EDV treatment which could be administered under the Australian Therapeutic Goods Administration (TGA) compassionate use scheme (ACTRN12617000037303; NHMRC Clinical Trials Centre, University of Sydney Australian New Zealand Clinical Trials Registry), which had been previously tested in a Phase I trial for mesothelioma (van Zandwijk et al., 2017) and recurrent glioblastoma (Whittle et al., 2015). P1 was dosed twice weekly for 7 weeks in her first cycle in the oncology ward at Royal North Shore Hospital, Sydney. However, because of her weakened state, and to potentially build tolerance to the lipopolysaccharide inherent in the EDV, doses were slowly escalated within the cycle. The dose were administered over 20 min via a 20 ml niki pump and premedication was given prior to dosing as before (van Zandwijk et al., 2017). Serum biochemistry, hematology and cytokine expression was evaluated pre and 3 hr post each dose. CA19-9 and C-reactive protein levels were monitored at least bi-weekly. Peripheral Blood mononuclear cells (PBMCs) were examined by flow cytometry (Gating strategy Figure S7) prior to dosing and at the end of the cycle for changes in antitumor immune cell numbers. Tumor tissue was obtained from the original surgical resection and PDAC cells were cultured and tested for drug sensitivity and surface receptors expression.

Clinical Trial

Clinical Trial NCT02766699 is a Phase 1 Study to Evaluate the Safety, Tolerability, and Immunogenicity of EGFR (Vectibix® Sequence)-Targeted EnGeneIC Dream Vectors Containing Doxorubicin (EGFR(V)-EDV-Dox) in Subjects with Recurrent Glioblastoma Multiforme (GBM). A 37-year-old Caucasian male presented with a two-month history of left lower extremity weakness, numbness, tingling, motor function change, difficulty walking, general weakness, fatigue, headaches and seizures and was diagnosed with glioblastoma (April 2017). The patient received 2 rounds of Temozolomide, right temporal lobe and right frontal lobe radiation, and Lapatinib. The patient was diagnosed with recurrent disease (August 2017) and recruited to the Cerebral EDV trial (ENG7) at Lennox Hill hospital in New York (NCT02766699; ClinicalTrials.gov Australian New Zealand Clinical Trials Registry). He was administered $8x10^9$ EGFR-EDV-Dox once a week in a 20 ml/20 min infusion for a 7-week cycle. Peripheral Blood mononuclear cells (PBMCs) were examined by flow cytometry prior to dosing and at the end of the cycle for changes in antitumor immune cell numbers.

In Vivo Tumor Models

All animal work was performed in accordance with the EnGeneIC animal ethics guidelines under AEC 1/2016, AEC 14/2016, AEC 15/2016, AEC 11/2017, and AEC 05/2019. For the 4T1 and CT26Ep12.1 model, female BALB/c mice were obtained from Animal Resources Centre at 6–8 weeks of age. For T84 and A549/DoxR models BALB/c nude mice were obtained from Animal Resources Centre at 5–7 weeks of age. After at least 1 week of observation, mice were injected with $5x10^4$ 4T1 cells per 50 μl PBS into the 3rd mammary fat pad on the right-hand side or $2x10^5$ CT26Ep12.1 per 100 μl PBS subcutaneously into the right flank of BALB/c mice. For human xenografts, $5x10^6$ A549/DoxR or $1x10^7$ T84 per 100 μl PBS/Matrigel (Sigma) was subcutaneously injected into the right flank. Treatment was commenced on day 7 post tumor induction for the 4T1 model, when the average tumor size was ~90 mm^3, and on day 9 for the CT26Ep12.1 model when the average tumor size was ~120 mm^3. Mice were treated via i.v, tail vein injection three times weekly for 2 weeks with one of the following treatments: Saline, $1x10^9$ EpCAM targeted EDVs (Ep-EDV), or $1x10^9$ EpCAM targeted EDVs loaded with PNU-159682 (Ep-EDV-682). Tumors were measured 3 times/week and tumor volume was calculated as π/6(Length x Width x Height). At the end of the 2 week period, mice were humanely euthanized, and tumors and spleens collected for *ex vivo* analysis. Treatment of A549/DoxR and T84 tumors was commenced when tumors reached 100-120 mm^3 and 120-150 mm^3 respectively. Mice were treated with Saline, $1x10^9$ EGFR targeted EDVs loaded with Doxorubicin (EGFR-EDV-Dox), $1x10^9$ EGFR targeted EDVs loaded with PNU-159682 (EGFR-EDV-682), or $1x10^9$ non-targeted EDVs loaded with PNU-159682 (EDV-682). For the survival and re-challenge study, treatment was commenced on day 7 in mice bearing CT26Ep12.1 tumor when tumors size was ~85 mm^3, and on day 3 in mice bearing 4T1 tumors when tumor sizes reached 30 mm^3. Mice received 4 doses of saline, $2x10^9$ Ep-EDV, or $2x10^9$ Ep-EDV-682 and then were monitored for tumor growth until

tumors reached 1000 mm^3, which was set as the survival ''endpoint''. All mice were re-challenged on day 15 (CT26Ep12.1) or day 11 (4T1) with an additional tumor inoculation on the opposite flank/mammary fat pad in addition to inoculation of a naive cohort. Spleens were collected from saline treated mice upon sacrifice as well as from surviving Ep-EDV-682 treated mice on day 50 post initial tumor inoculation for flow cytometric analysis of memory T cell populations.

METHOD DETAILS

EnGeneIC Dream Vector (EDV)

EDV were produced and purified from a *Salmonella enterica serovar Typhimurium* (*S*. Typhimurium) *min*CDE- strain as previously described (MacDiarmid et al., 2007b). Drug loading, antibody targeting, lyophilization, and dose preparation have been previously described (MacDiarmid et al., 2007b; Sagnella et al., 2018). EDV preparations were subject to strict quality control in which EDV size and number were assessed using dynamic light scattering using a Zetasizer Nano Series and NanoSight LM20 (Malvern Instrument). Endotoxin levels were assessed using an Endosafe portable test system (Charles River). Drug was extracted from EDV^{TM} preparations and quantified via HPLC as previously described (MacDiarmid et al., 2007b).

Flow Cytometry

All flow cytometry was performed on a Beckman Coulter Gallios 6C.

Cell Culture

RAW264.7 cells (ATCC) were grown to ~70% confluence in Dulbecco's Modified Eagle Media (DMEM) (Sigma) containing 10% FCS and passaged using a cell scraper. Mouse tumor cell lines (4T1 and CT26) were grown in monolayers in RPMI-1640 media (Sigma) containing 10% FCS and passaged 2-3 times per week using phosphate buffered saline (PBS)/Trypsin EDTA. All cells were maintained in culture at 37°C in a humidified atmosphere containing 5% CO_2 and routinely screened and found to be free of mycoplasma. EpCAM expression and receptor number in the mouse cell lines was quantified using flow cytometry with APC anti-mouse CD326 (Biolegend) using Quantum Simply Cellular anti-Rat IgG microspheres (Bangs Laboratory). As CT26 were shown to be negative for EpCAM, cells were transfected with a pcDNA3.1+C DYK vector containing the mouse EpCAM ORF clone (NM_008532.2) (Genescript) using Lipofectamine 2000 (Thermo Fisher). G418 selection was used to obtain pure populations of EpCAM expressing CT26 clones, and cells were screened as described above for EpCAM expression. Clones were examined for growth rate, drug sensitivity and *in vivo* tumorgenicity, and one that possessed high EpCAM expression with the above 3 parameters being similar to the parental CT26 cell line was selected for all subsequent studies (CT26Ep12.1).

Bone Marrow Derived DCs (BMDC)

Bone marrow was isolated from the femurs and tibias of BALB/c mice. Following red blood cell lysis and washing, cells were resuspended in AIMV + 5%FBS +2-mercaptoethanol +penicillin/streptomycin +20 ng/ml GM-CSF (Miltenyi Biotec) and grown for 7 days.

Treatment of RAW264.7 Cells with EDVs

RAW264.7 cells were seeded in 6-well plates at 3×10^5 cells per well and incubated overnight. Media was then replaced with fresh media containing one of the following: 1 μg/mL LPS (Sigma); 100 pmol PNU-159682 (Najing Levena); Ep-EDV-682 (500:1 and 1000:1 EDV: cells), Ep-EDV (5000:1 EDV: cells) or left untreated. Cells were harvested 6 hr and 24 hr post treatment using a cell scraper and samples were stained with DAPI (Sigma), anti-CD45 Brilliant Violet 510 (BioLegend), anti-CD86 APC-Cy7 (BioLegend), and anti-CD206 AF488 (R&D Systems) and assessed by flow cytometry.

Macrophage and DC/Tumor Cell Co-cultures

CT26Ep12.1 and 4T1 cells were harvested with Versene (Gibco) and cells were collected in 1 mL Eppendorf tubes. Cells were resuspended in 1 mL DMEM (Sigma) supplemented with 10% FBS (Bovogen) containing: Ep-EDV (1000:1 and 5000:1 - EDV: cells); Ep-EDV-682 (500:1 and 1000:1- EDV: cell); Ep-EDV-Dox (10,000:1 – EDV: cell), 100 pmol PNU-159682, 5 μM Doxorubicin, or media alone. Drug and EDV amounts were established via MTS and xCELLigence real time experiments such that chosen concentrations resulted in the initiation of cell death within the first 24 hr post treatment. Cells were then washed thoroughly with PBS to remove any non-adherent EDV or excess drug. Treated tumor cells were cultured overnight with either RAW264.7 or BMDC at a 1:1 ratio of tumor cells: RAW264.7/BMDC. Supernatants were collected for ELISA analysis. RAW264.7/tumor cell co-cultures were collected using a cell scraper and samples were stained with DAPI (Sigma), anti-CD45 Brilliant Violet 510 (BioLegend), anti-CD86 APC-Cy7, and anti-CD206 AF488 and assessed by flow cytometry. BMDC/tumor cell co-cultures were collected with versene and stained with DAPI (Sigma), CD11b AF488 (Abcam), CD11c PE (Molecular Probes), anti-CD45 Brilliant Violet 510 or PECy5 (BioLegend), anti-CD86 APC-Cy7, MHC Class II PECy5 (Thermo Fisher), MHC Class II Brilliant Violet 421 (BioLegend), 7-AAD (BioLegend), and/or CD80 PE (Thermo Fisher) and assessed by flow cytometry. RNA was extracted from BMDC/tumor cell co-cultures using an RNAeasy Plus Mini Kit (Qiagen) according to the manufacturer's protocol. Briefly, cells were lysed and homogenized in RLT buffer, and passed through a gDNA eliminator spin column. 70% ethanol was added to the flow through and samples were then passed through a RNeasy spin column, washed and eluted in RNase-free water. RNA concentration was determined on an Eppendorf biophotometer plus. The RNA was used to reverse transcribe cDNA using a SuperScript^{TM}VILO^{TM}cDNA Synthesis Kit (Thermo Fisher) according to

the manufacturer's protocol. The transcribed cDNA was diluted 1:2 for qPCR. Each qPCR reaction contained 5 μL TaqMan fast advanced master mix (Thermo Fisher), 0.5 μL 20X Taqman primer/probe mix (IFNα Mm03030145_gH, IFNb1 Mm00439552_s1, GAPDH Mm99999915_g1; Thermo Fisher) and 2.5 μL of water. 8 μL of the mix plus 2 μL of cDNA was added into a 96 well plate. qPCR was performed using an Applied Biosystems Real-Time PCR System. Data was exported to excel, and the relative quantitation was calculated from the ΔΔCt.

In Vivo Immune Cell Depletion

After CT26Ep12.1 tumors reached an average size of 110-120 mm^3, mice were injected with 100 μg *In VivoMAb* anti-mouse/human CD11b (M1.70) (BioXCell), 300 μg *InVivoPlus* anti-mouse CD8α (2.43) (BioXCell), 300 μg *InVivoPlus* anti-mouse CD4 (GK1.5) (BioXCell), 50 μl Ultra-LEAF purified anti-Asialo-GM1 (Biolegend), or 100 μl clodronate liposomes (Liposoma Research) 24 hr prior to commencing EDV treatment. Preliminary studies indicated ~75% splenic depletion of $CD11b^+$ cells which occurred within 24 hr of Anti-CD11b administration, ~80-85% splenic depletion of NK cells within 24 hr of Anti-Asialo-GM_1 administration, >99% splenic depletion of CD4/CD8 T cells within 24 hr of Anti-CD4/CD8 $_1$ administration, and >94% splenic depletion of macrophages within 24 hr of clodronate liposome treatment. Depletion in tumors achieved similar levels. To maintain depletion levels, anti-CD11b and clodronate liposomes were administered every 4 days, while anti-CD4, anti-CD8α, and anti-Asialo were administered weekly.

Isolation of $CD11b^+$ Cells from 4T1 and CT26Ep12.1 Tumor

Tumors were dissected, weighed, and enzymatically digested using a Tissue Dissociation Kit (Miltenyi Biotec) at 37°C according to the manufacturer's instructions, using the gentleMACS™ Dissociator. Following dissociation, red blood cells were removed using RBC lysis buffer (Sigma). After washing, cells were passed through a 70 μm cell strainer to remove any clumps. $CD11b^+$ cells were purified by positive selection using CD11b MACS beads (Miltenyi Biotec) on a LS column on the MACS separator (Miltenyi Biotec). The purity of the isolated $CD11b^+$ cell population was assessed by flow-cytometry with an APC anti-mouse CD11b (Biolegend) and shown to be ~80% pure (Figure S8A).

Isolation of NK and CD8 from Spleens

Spleens were homogenized using a Dounce homogenizer and filtered through 70 μM mesh strainers to obtain single cell suspension followed by erythrocyte lysis using RBC lysis buffer. Splenocytes were then washed and a cell count performed before progressing to NK or $CD8^+$ T cell isolation. NK cells and $CD8^+$ T cells were isolated from dissociated spleen cells by negative selection using either the NK Cell Isolation II kit (Miltenyi Biotec) or the $CD8a^+$ T Cell Isolation Kit (Miltenyi Biotec), according to the manufacturer's instructions. Cells were separated by using a LS column on the MACS separator (Miltenyi Biotec). NK cell and $CD8^+$ T cell preparations were assessed by flow-cytometry and NK cell purity was consistently greater that 90% (Figure S8B) while $CD8^+$ T cell purity was consistently greater than 86% (Figure S8C). NK cells were rested overnight in RPMI-1640 media supplemented with 10% FBS at 37°C prior to the NK cell-mediated cytolysis assay. $CD8^+$ T cells were added to tumor cells immediately following isolation to assess $CD8^+$ T cell cytolysis.

xCELLigence Monitored $CD11b^+$, $CD8^+$, and NK Cell Cytolysis of Tumor Cells

Cell growth characteristics and tumor cell death were monitored in real time by the xCELLigence DP system. To do so, circular electrodes covering the base of the tissue culture wells detect changes in electrical impedance and convert the impedance values to a Cell Index (CI). Cell Index measurements directly correspond to the strength of cell adhesion, cell speading, and cell number. Target cells (4T1, CT26Ep12.1, A549/DoxR, or T84) were seeded into an E-Plate 16. Cells were left to attach and proliferate until they had reached their logarithmic growth phase. The effector cells ($CD11b^+$ cells, NK cells, or $CD8^+$ T cells) were added to the target cells at the following effector-to-target cell ratios: 5:1 ($CD11b^+$: tumor cell), 20:1 (NK cell: mouse tumor cell), 10:1 (NK:human tumor cell), and 30:1 ($CD8^+$ T cell: tumor cell). After addition of effector cells, the system took regular measurements (every 5 or 15 min) for 3-4 days to monitor immune cell-mediated killing of tumor cells.

NK Cell Mediated Cytolysis Inhibition

Mouse tumor cell lines were initially screened for NK cell ligand expression via flow cytometry with anti-Rae-1α/β/γ-PE (Miltenyi Biotec), anti-H60a-PE (Miltenyi Biotec), and anti-MULT-1 PE (R&D Systems). For NK cell-mediated cytolysis inhibition based on these ligand expression levels, the effector NK cells were added to target cells in the presence of 3 μg/ml of blocking mAb to the following NK cell ligands: anti-RAE-1αβγ (R&D Systems) or anti-H60 (R&D Systems) separately and as a mixture.

Tumor/Spleen Flow Cytometry

Tumors and spleens were dissociated as described above. Following red blood cell lysis, cells were incubated with Fc block 1:10 in MACS buffer (Miltenyi Biotec) for 10 min. After the 10 min incubation, cells were washed once and incubated with a primary antibody panel in MACS buffer for 15 min on ice in the dark. Cells were washed 2 times and then resuspended in MACS buffer for flow cytometric analysis. The following antibodies were used in T cell, NK cell, and macrophage staining panels: anti-CD45 PECy7 (BioLegend), anti-CD45 BV510 (Biolegend), anti-CD45 APC/Fire750 (Biolegend), anti-CD3e APC-eFluor780 (eBioscience), anti-CD3 APC (Molecular Probes), anti-CD4 PE-TR (Abcam), anti-CD4 PE-TR (RM4-5; Molecular Probes), anti-CD8a FITC (eBioscience), anti-CD8 BV510 (BioLegend), anti-CD8b FITC (Biolegend), anti-CD25 PE (Abcam), anti-CD314 (NKG2D) PE-eFluor610 (eBioscience),

anti-CD335 (NKp46) PECy7 (BioLegend), anti-CD27 BV421 (BioLegend), ant-CD183 (CXCR3) BV510 (BioLegend), anti-NKG2A/C/E FITC (eBioscience), anti-CD11b APC (BD Pharmingen), anti-CD11b APC (3A33; Southern Biotech), anti-CD49b APC-eFluor780 (eBioscience), anti-Ly6C FITC (BioLegend), anti-Ly6G BV510 (BioLegend), anti-F4/80 PE Dazzle594 (BioLegend), anti-CD206 PECy7 (BioLegend), and anti-CD86 APC-Cy7 (BioLegend). For the memory T cell panel, the mouse naive/memory T cell ID panel (Biolegend) was used in conjunction with anti-CD8 BV510 (Biolegend). Single stained controls and/or versacomp (Beckman Coulter) beads were used for fluorescence compensation. DAPI (Sigma), propidium iodide (Sigma), DRAQ5 (Thermo Fisher), 7-AAD (Biolegend), or Live/Dead Yellow (Thermo Fisher) were used for live cell detection. Unstained and isotype controls were employed to determine auto-fluorescence levels and confirm antibody specificity.

Cytokine and Chemokine Detection

To measure the interstitial cytokine and chemokine levels in the mouse tumors, tumors were carefully dissected removing all skin, placed into serum free media, and weighed. Tumors were then gently broken up using Eppendorf micropestles (Sigma), ensuring no large pieces were visible. The cell suspension was centrifuged, and the supernatant collected and stored at -80°C until analysis. Tumor supernatant was analyzed for mouse IL-1β, TNF-α, IL-2, IL-4, IL-6, IL-12p40, IFNα, IFNγ, CCL2, CCL3, and CCL5 according the manufacturer's instructions. The IFNα kit was obtained from PBL Assay Science, while IL-1β, TNF-α, IL-2, IL-4, IL-6, IL-12p40, IFNγ, RANTES (CCL5), MIP-1α (CCL3), and MCP-1 (CCL2) duoset kits were obtained from R&D systems. Each ELISA was developed using the 3,3',5,5'-tetramethylbenzidine (Sigma) substrate. Microwell plates were read in a Biotek uQuant plate reader at 450 nm with 540 nm as the reference wavelength.

QUANTIFICATION AND STATISTICAL ANALYSIS

Flow Cytometry

All flow cytometry was analyzed using Kaluza software (Beckman Coulter).

Cytokine and Chemokine Detection

KC junior software was used to fit 4 parameter logistic curves to the standards and interpolate the samples. The minimum detectable concentration (MDC) of each assay was calculated by multiplying the s.d. of the response by 10 and dividing by the slope of the standard curve at the inflection point.

Statistics

All statistical analysis was performed using the GraphPad Prism software package. Data is represented as mean ± standard deviation (SD) or standard error of the mean (SEM). Statistical significance between 2 groups was determined by a student's t-test. Statistical significance between groups of 3 or more was determined by a one-way or two-way ANOVA, followed by the Tukey's multiple comparison test. Significance for tumor regression studies was determined by a two-way ANOVA followed by the Tukey's multiple comparison test. For all tests, p values were as follows: * $p \leq 0.05$, ** $p \leq 0.01$, *** $p \leq 0.001$, and **** $p \leq 0.0001$.

DATA AND CODE AVAILABILITY

This study did not generate any unique datasets or code.